ACS Energy LETTERS
ACS EDITORS' CHOICE
http://pubs.acs.org/journal/aelccp

Solar-Driven Metal Halide Perovskite Photocatalysis: Design, Stability, and Performance

Haowei Huang, Bapi Pradhan, Johan Hofkens, Maarten B. J. Roeffaers,* and Julian A. Steele*

Cite This: *ACS Energy Lett.* 2020, 5, 1107−1123 Read Online

ACCESS | Metrics & More | Article Recommendations

ABSTRACT: The development of green, sustainable, and economical chemical processes represents a cornerstone challenge within chemistry today. Semiconductor heterogeneous photocatalysis is currently utilized within a wide variety of societally impactful processes, spanning reactions such as hydrogen production and CO_2 conversion, to the organic transformation of raw materials for value-added chemicals. Metal halide perovskites (MHPs) have recently emerged as a new promising class of cheap and easy to make photocatalytic semiconductors, though their unstable ionically bound crystal structure has thus far restricted widespread application. In this Review, we examine the issues hampering MHP-based photocatalysis and highlight the general approaches being taken to achieve promising and stable photocatalytic reaction environments. Specifically, we outline the adoption of (1) halogen acid solutions (i.e., HX; X = I or Br) for hydrogen evolution reactions, (2) relatively low-polarity solvents for CO_2 photoreduction and organic transformations, and (3) the encapsulation of perovskites for CO_2 reduction and water splitting. Further, we detail the measures being taken to arrive at intrinsically stable photocatalytic materials, removing the need for atypical environments. With each technology offering unique sets of benefits and challenges, we conclude by outlining potentially promising opportunities and directions for metal halide perovskite-based photocatalysis research moving forward.

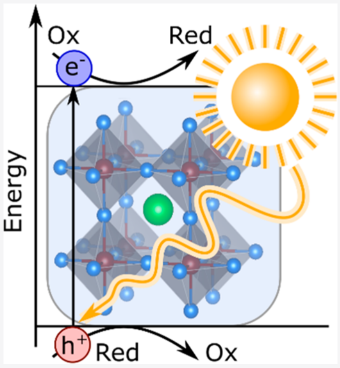

Like the natural and efficient energy conversion exhibited by photosynthesis, photocatalysis presents an effective way for man-made solar-to-chemical energy conversion.[1,2] The first report of UV-driven photocatalytic hydrogen production on TiO_2 in 1972[3] has since motivated decades of scientific exploration and development, leading to several applications important for human society; from energy conversion (e.g., water splitting, CO_2 reduction) and chemical transformations, to the remediation of organic pollutants. Reactions driven by photocatalytic materials generally follow three separate processes: (i) absorption of photons to generate electron and hole pairs, (ii) charge separation and migration to reaction sites on the photocatalyst surface, and (iii) chemical oxidation and reduction at the surface mediated by the photogenerated holes and electrons, respectively.[4]

An ideal photocatalytic material should embody several desirable physical traits, namely, broad and strong light absorption, efficient charge separation, long operational stability, and the appropriate redox ability for target reactions.[5] In reality, however, most photocatalysts are far from perfect. For example, pristine TiO_2, graphitic carbon nitride (g-C_3N_4), and $BiVO_4$ have their own shortcomings such as wide bandgap,[6] rapid recombination of photogenerated charge carriers,[7] and poor photoreduction potential,[8] respectively. It follows that a strong desire to develop new semiconductor photocatalysts with suitable properties continues to motivate intense materials exploration and research within the field.

Metal halide perovskite (MHP) semiconductors have recently emerged as promising optoelectronic materials for applications spanning efficient solar cells and LEDs, to lasers and photodetector devices.[21] MHPs are ionic crystals with the general chemical formula ABX_3. Here A is a monovalent cation (MA: $CH_3NH_3^+$, FA: $CH(NH_2)_2^+$ and Cs^+); B represents a divalent metal cation (Pb^{2+}, Sn^{2+}, or Cu^{2+}), and X is a halogen anion (Cl^-, Br^-, or I^-).[22] The successful application of MHPs within optoelectronic devices is driven mainly by their low production costs and easy solution processing;[22] tunable, direct bandgap;[23,24] long carrier diffusion lengths;[25] high carrier mobility;[26] and unusual tolerance to defects.[27] Compared to

Received: January 8, 2020
Accepted: March 6, 2020
Published: March 6, 2020

ACS Publications

https://dx.doi.org/10.1021/acsenergylett.0c00058

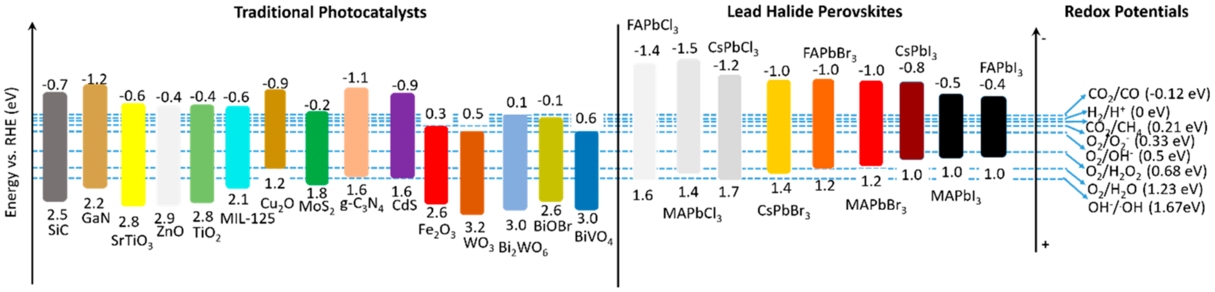

Figure 1. Band edge positions of conventional photocatalysts and different MHPs relative to reversible hydrogen electrode (RHE).[6−16] For comparison, the redox potential of some common half-reactions are also presented.[17−20]

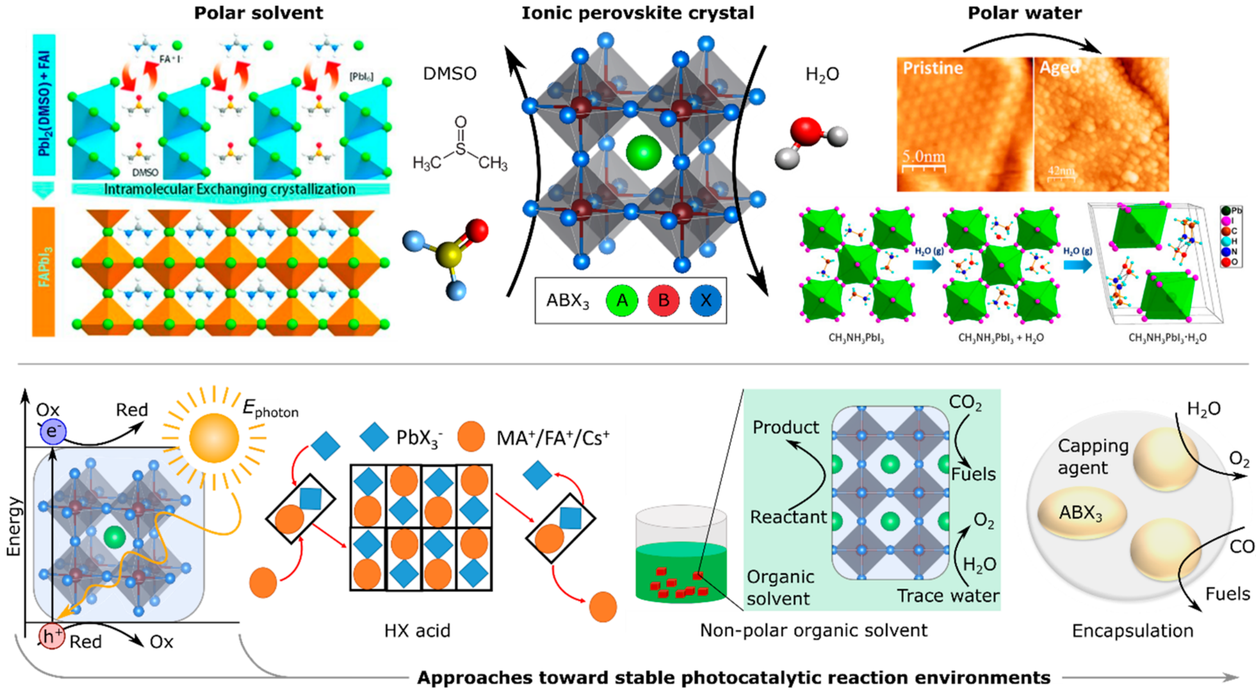

Figure 2. Top: Illustration of the vulnerability of MHP surfaces during photocatalytic reactions, when exposed to polar solvents (e.g., DMSO) and water.[31−33] Polar molecules undergo rapid intramolecular exchange with the organic cation, causing the immediate degradation of the perovskite chemical structure. Water molecules degrade MHPs in a stepwise fashion, where initially a monohydrate perovskite structure is formed which later decomposes into nonperovskite structures, through different intermediates. Reproduced with permission from ref 31. Copyright 2015 The American Association for the Advancement of Science. Reproduced from refs 32 and 33. Copyright 2016 American Chemical Society. Bottom: Three main routes toward creating stable reaction environments when employing MHPs as a photocatalyst: saturated haloacid solutions stabilize MHPs by establishing a dynamic ionic equilibrium between the dissolved ionic species and the solid perovskites; nonpolar or relatively low-polarity solvent dispersion reduces the degradation pathways; and encapsulation via capping agents or shelling prevents direct contact with polar solvents or reaction products.

more traditional photocatalysts, MHPs exhibit relatively narrow bandgap energies as shown in Figure 1, enabling the absorption of lower-energy solar photons.

Based on the reaction thermodynamics, a suitable match is required between the electronic band structure of a semiconductor and reaction redox potential. The potentials of typical photocatalytic half-reaction involved in water splitting, CO_2 reduction, aerobic organic transformation, and dye degradation are shown in Figure 1.[20] Here, the relative position of the MHP conduction band (CB) and valence band (VB) are depicted alongside these redox potentials. Based on their comparison, Figure 1 highlights the excellent reduction ability of MHPs; that is, the relative position of their CB is typically negative enough for H_2 generation, CO_2 reduction, superoxide radical generation. Additionally, some members of the MHP family (namely the Cl-based materials and all-inorganic $CsPbBr_3$) can in theory also achieve water oxidation, because of their relatively positive valence band maximum (VBM). For hydroxyl radical formation, which is often involved in dye degradation, the required potential is above the VBM of MHPs, making them an unsuitable candidate.

Considering the (photo)physical properties exhibited by MHPs, they seemingly satisfy several of the important requirements for good photocatalytic reactions as shown in Figure 1. Indeed, the first report of MHP-based photocatalysis appeared as recently as December 2016, where Nam and coworkers[28] outlined a strategy for photocatalytic-driven HI splitting using $MAPbI_3$, exploiting the dynamic equilibrium of the dissolution and reprecipitation of $MAPbI_3$ in saturated HI aqueous solutions. This particular approach proved effective, as the ionic lattice of MHPs is highly unstable under more typical photocatalytic reaction conditions. For example, H_2O splitting,

CO_2 and N_2 reduction, and dye degradation all require water or a polar solvent, which facilitate degradation pathways detrimental for long-term use (Figure 2).[29,30] Furthermore, for some radical-based reactions, like dye degradation, water or polar solvents are prerequisite for the formation of the radical species that drive the reaction forward. Within this context, it is the relatively reactive and unstable nature of ionic MHP crystals which has thus far limited their application as a photocatalyst. In this Review, the current prospects of effectively applying MHPs in photocatalysis are discussed. We provide a critical analysis of the instability issues hampering progress in this new branch of scientific research and highlight proven strategies allowing for stable reaction environments. Finally, a brief perspective on the future challenges and possibilities of this promising new technology are described.

Instability Constraints in MHP Photocatalysts. The structural and optoelectronic properties of MHPs change significantly upon phase transitions, thermal stress, ambient air exposure (oxygen and moisture), and illumination (UV light). The ionic interactions binding the charged components of MHP crystals render them vulnerable to structural modifications at its surface when coming into contact with polar additives. This particular feature within MHPs defines the limited scope of photocatalytic reactions for which these semiconductors have been effectively applied. As shown in Figure 2, MHPs tend to decompose relatively quickly into a PbX_2 (X = I, Br, Cl) precipitate, Cs^+/MA^+/FA^+ cations, and halide anion when exposed to polar molecules. The volatile nature of hygroscopic amine salts, the MA^+, FA^+ cations contained in hybrid organic−inorganic MHPs, leads to moisture instability.[34−39] Also in Figure 2, water interacts with the crystal via hydrogen bonding to hydrate the surface, yielding a polycrystalline nonperovskite structural coating and grain boundaries.[33]

The quantitative and systematic investigation of the humidity-induced structural and chemical degradation mechanism of $MAPbI_3$ has been performed by ultrafast transient absorption spectroscopy and kinetics studies,[35] *in situ* grazing incidence X-ray diffraction,[36] and via ab initio molecular dynamics simulations.[37] The absorbed water molecules easily penetrate the MHPs structure and form intermediate monohydrate and dihydrate structures by reacting with the $[PbX_6]^{4-}$ octahedral units.[32] This is followed by rapid material breakdown through hydrolyzation (eqs 1−4):[30,35−39]

$$CH_3NH_3PbI_3 + H_2O \rightarrow CH_3NH_3PbI_3\cdot H_2O \quad (1)$$

$$4CH_3NH_3PbI_3 + 2H_2O \rightarrow (CH_3NH_3)_4PbI_6\cdot 2H_2O + 3PbI_2 \quad (2)$$

$$CH_3NH_3PbI_3\cdot H_2O \rightarrow PbI_2 + CH_3NH_3I + H_2O \quad (3)$$

$$CH_3NH_3I \rightarrow CH_3NH_2 + HI \quad (4)$$

The hydrogen bond between the organic and inorganic units is one of the key features in stabilizing the perovskite structure and is compromised through this process; water forms two new types of hydrogen bonds, a strong one with the lattice halides and another one weakly with the organic cations.[30,40,41] Notably, the interaction between MA and H_2O is not established until the monohydrate phase transition, where the two become locked.[32] In polycrystalline thin films, the monohydrate phase formation occurs independently of the film thickness because of the rapid transport of water molecules across grain boundaries.[32] Even in bulk $MAPbI_3$ single crystals, aging under ambient conditions shows prominent surface restructuring with the formation of grain boundaries.[33] This is a direct consequence of the surface undergoing rapid hydration upon exposure to moisture, relative to the shielded interior. Furthermore, light absorption in MHPs initiates a halide-to-metal charge-transfer process which reduces the charge density at the X sites, thereby weakening the $CH_3NH_3\cdots X$ hydrogen bonding interactions and causing an increased rate of degradation upon illumination under a humid atmosphere.[42]

As shown in Figure 2, when MHPs are exposed to polar solvents like dimethyl sulfoxide (DMSO), the perovskite structure also degrades to form coordination compounds, such as $PbI_2(DMSO)_2$, MAI-PbI_2-DMSO via van der Waals interactions.[31,43,44] Rapid intramolecular exchange between DMSO and FAI in $FAPbI_3$ causes immediate decomposition of the perovskite structure. Solution-processed perovskite thin films possess much more prominent defects when they are fabricated from a polar coordinating solvent (e.g., DMF, DMSO, γ-butyrolactone), relative to the noncoordinating polar solvents (e.g., acetonitrile).[45] This arises from the tendency of coordinating solvents to get intercalated more easily during the perovskite film formation.

The photostability of MHPs in the presence of ambient oxygen (O_2) is also low. Reports have shown that iodide-based perovskites (i.e., $MAPbI_3$) break down under simulated solar irradiation (AM 1.5G) and O_2 exposure.[46,47] This process is mediated by the rapid generation of iodide vacancies upon photoexcitation, which offers a pathway for oxygen to be introduced into the MHPs crystal lattice. Molecular oxygen reacts with photogenerated electrons at the iodide vacancy sites, producing reactive superoxide species which subsequently react with MA cation, resulting in water, methane gas, and lead iodide as the decomposition products.[47,48]

The lattice of MHP semiconductors is increasingly being considered as soft in nature because of the occurrence of several structural and chemical dynamic effects. Ultimately, the soft nature exhibited by MHP crystals renders their surfaces prone to structural modification and degradation as discussed above. The replacement of A site organic cations with inorganic Cs^+, resulting in the formation of all-inorganic chemical structure, substantially increases resistance to humidity and photostability.[49,50] The ionization energy of Cs compared to MA can explain the higher chemical stability of the all-inorganic perovskites.[51] For example, $CsPbBr_3$ nanocrystals are found to be substantially more stable in polar solvents, e.g., isopropyl alcohol, ethyl acetate, methyl acetate, acetonitrile, which is encouraging for a vast number of photoredox catalysis reactions.[52]

The instability issues outlined above have motivated the development of several approaches aimed toward realizing stable photocatalytic environments, which are summarized at the bottom of Figure 2: (i) placing MHPs in saturated halo acid solutions for solar-driven water splitting,[28,53−61] (ii) minimizing direct contact with highly polar environments via targeted low-polarity solvents and solutions,[62−80] and (iii) encapsulating MHP nanocrystals to screen them from polar molecules.[81−95] Efforts are also being made toward realizing MHPs which are intrinsically stabilized against exposure to polar solvents. Currently, some all-inorganic MHPs have proven to be stable in polar solvents.[96−102] In what follows we outline the current state of play for each of these approaches, highlighting their successes and pitfalls and the features which ultimately govern their realistic potential.

https://dx.doi.org/10.1021/acsenergylett.0c00058
ACS Energy Lett. 2020, 5, 1107−1123

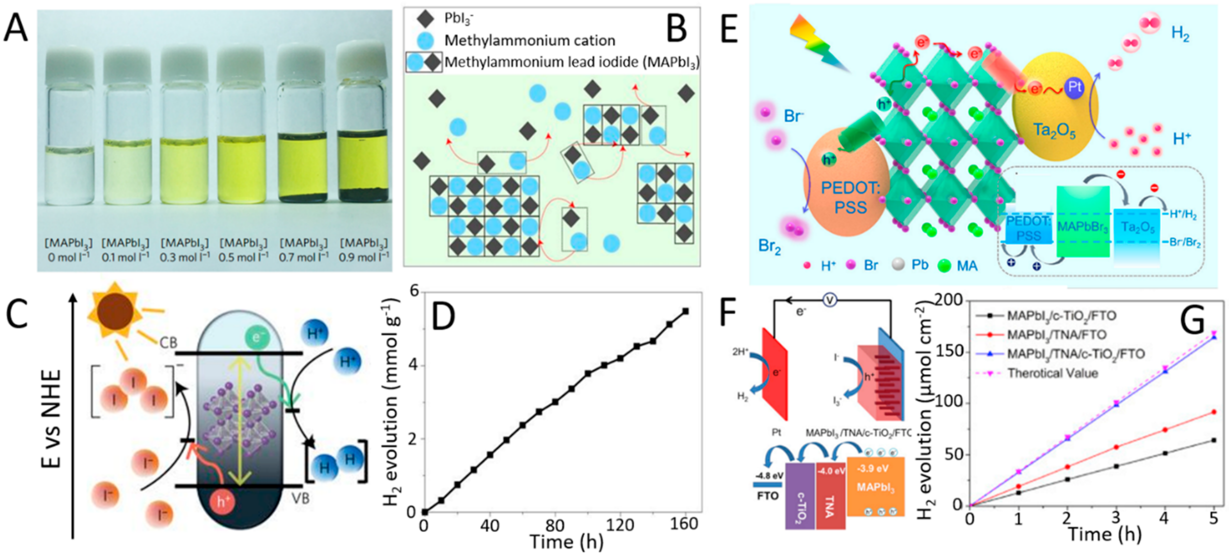

Figure 3. (A) $MAPbI_3$ in aqueous HI solutions at different concentrations, (B) scheme representing the equilibrium between $MAPbI_3$ dissolution and recrystallization in a saturated HI solution, (C) band diagram of the $MAPbI_3$ powder for the HI splitting photocatalytic reaction, and (D) stable photocatalytic H_2 evolution in the saturated solution for 160 h.[28] Reproduced with permission from ref 28. Copyright 2017 Springer Nature. (E) Reaction mechanism for $MAPbBr_3$ with Pt/Ta_2O_5 and PEDOT:PSS as the electron- and hole-transporting motifs, respectively, for photocatalytic HBr splitting reaction, and the corresponding energy level diagrams of $MAPbBr_3$, Ta_2O_5, and PEDOT:PSS.[56] Reproduced from ref 56. Copyright 2019 American Chemical Society. (F) Scheme of charge transfer in photoelectrochemical HI splitting cell of $MAPbI_3$/TNA(TiO_2 nanorod array)/c-TiO_2/FTO (F doped SnO_2) photoelectrode as the band alignment, and (G) the H_2 evolution on this cell for 5 h.[58] Reproduced with permission from ref 58. Copyright 2019 Elsevier.

Saturated Haloacid Solutions. Because MHPs are water-soluble ionic compounds, utilizing the precipitation−solubility equilibrium between the perovskite phase and the soluble ionic species is a creative approach to solve the stability problem. Nam et al.[28] first introduced the photocatalytic H_2 production in methylammonium lead iodide ($MAPbI_3$) saturated hydrogen iodide (HI) acid aqueous solution using $MAPbI_3$ perovskite polycrystalline powders. As shown in Figure 3A,B, in a saturated HI solution, micrometer-sized $MAPbI_3$ particles dissolve to form methylammonium cations and PbI_x complex anions, with an equal amount of $MAPbI_3$ particles recrystallizing in parallel. The $MAPbI_3$ phase would be largely modulated by the I^- and H^+ ion concentrations in the aqueous solution. In a relatively high ion concentration regime (>3.16 mol/L HI solution), together with a lower iodide concentration (i.e., $[I^-] \leq [H^+]$, whereby $HClO_4$ is added), the $MAPbI_3$ perovskite phase remained stable. Figure 3C presents the reaction mechanism for photocatalytic HI splitting on $MAPbI_3$. Upon irradiating with visible light ($\lambda \geq$ 475 nm), these mixtures produced roughly 26 μmol of H_2 in 9 h using $MAPbI_3$ as a photocatalyst, with the photogenerated holes driving the I^- to I_3^- oxidation. In addition, as a good reducing agent of I_3^- to I^-, H_3PO_2 was added to maintain the I^- concentration. Because of the dynamic equilibrium between the $MAPbI_3$ powders and the ionic species in the saturated solution, $MAPbI_3$ remained stable for 160 h under continuous irradiation, without any compromise to the activity as shown in Figure 3D. Furthermore, the deposition of Pt on the $MAPbI_3$ (i.e., Pt/$MAPbI_3$) increased the hydrogen evolution rate to 57 μmol/g/h, resulting in a solar-to-chemical conversion efficiency (the ratio of solar light converted to chemical energy) of 0.81%. In the Pt/$MAPbI_3$ sample, as the $MAPbI_3$ particles dissolve and reprecipitate, the change in contact between $MAPbI_3$ and Pt is unclear.

In a similar fashion, Li et al.[57] improved the photocatalytic activity of Pt/$MAPbI_3$ by inserting TiO_2 between Pt and $MAPbI_3$. The Pt/TiO_2-$MAPbI_3$ photocatalyst powders, based on micrometer-sized $MAPbI_3$ displayed a nearly 90-fold enhancement for H_2 generation (ca. 7.3 mmol/g/h,) from aqueous HI solution compared to the parent Pt/$MAPbI_3$ (ca. 830 μmol/g/h) system. The introduction of TiO_2 not only improved the extraction of electrons from $MAPbI_3$ via suitable band alignment but also acted to stabilize the Pt cocatalyst. The approach of Huang et al.[53] was similar, in that they modified $MAPbI_3$ bulk microcrystals with reduced graphene oxide (rGO) to efficiently extract electrons from the $MAPbI_3$ light absorber, as well as provide H_2 release sites. The combined $MAPbI_3$/rGO system exhibited an H_2 evolution rate of 939 μmol/g/h, which is 67 times greater than that of pure $MAPbI_3$. After 200 h of irradiation, the composite material remained stable and did not display decreased photocatalytic activity.[53] Zhao et al. also used rGO to extract the photogenerated electrons, this time from a lead-free "double perovskite" ($A_2{}^{I}B^{I}B^{III}X_6$ architecture) $Cs_2AgBiBr_6$ bulk photocatalyst. In saturated HBr and H_3PO_2 solution, a 48.9 μmol/g/h H_2 release rate was achieved on $Cs_2AgBiBr_6$/rGO composite with visible light irradiation, which is 80 times greaterer than that of pure $Cs_2AgBiBr_6$.[61] Chen et al. similarly modified $MAPbI_3$ bulk microcrystals for photocatalytic applications, though with black phosphorus (BP).[59] The BP/$MAPbI_3$ system offered an impressive H_2 evolution rate of 3472 μmol/h/g in HI solution. Widening the fundamental bandgap with bromine atoms at the halide sites, Li et al. demonstrated that $MAPbBr_3$ bulk microcrystals can be used for steady photocatalytic H_2 production in saturated $MAPbBr_3$ aqueous HBr solution upon visible light irradiation.[56] Their perovskite semiconductors were further modified with PEDOT:PSS (poly(3,4-ethylenedioxythiophene) polystyrenesulfonate) and Ta_2O_5 as cocatalysts, preparing PEDOT:PSS/$MAPbBr_3$/Ta_2O_5. As described in Figure 3E, because of band alignment of PEDOT:PSS and Ta_2O_5 with $MAPbBr_3$, these additives acted as hole and electron transporting layers, respectively, for efficient photogenerated charge separation. Notably, in comparison to the pure $MAPbBr_3$, ca. 52 times enhancement of the hydrogen evolution rate was achieved with the hybrid material, and an apparent quantum efficiency ($AQE = N_{electron}/N_{photon}$) of ca. 16.4% was reported for 420 nm excitation. However, the photocatalytic activity of this hybrid material decreased gradually within a 4 h time experiment. The instability of this system comes from the agglomeration of PEDOT:PSS in the reaction solution, thus affecting the interfacial charge transfer between $MAPbBr_3$ and PEDOT:PSS. Finding a more suitable hole transport material to replace PEDOT:PSS could give rise to the high efficiency and stable photocatalytic production of H_2.

Huang et al. introduced iodine into hybrid $MAPbBr_3$ and all-inorganic $CsPbBr_3$ bulk microcrystals (i.e., $MAPbBr_{3-x}I_x$[54] and $CsPbBr_{3-x}I_x$[55]) to form bandgap funnel structures via the graded distribution of I atoms. In saturated HBr/HI mixed acid solution, both the $MAPbBr_{3-x}I_x$/Pt and $CsPbBr_{3-x}I_x$/Pt photocatalysts exhibited decent H_2 evolution under visible light irradiation, reaching 2604.8 μmol/g/h and 1120 μmol/g/h, respectively. Furthermore, both samples displayed a high stability during the 50 h of testing. A similar strategy was followed for lead-free perovskite $MA_3Bi_2I_9$ with a lamellar structure, as the system reaches a precipitation−solubility equilibrium in saturated HI solution.[60] The photocatalytic rate for H_2 evolution on Pt/$MA_3Bi_2I_9$, with Pt as cocatalyst, is nearly 170 μmol/g/h in saturated HI solution. After 70 h of cycling, no decrease in H_2 evolution rate was observed for this catalyst.

The band engineering strategy for MHPs stabilized within a halogen acid solution was further developed by Liu et al., with the photocatalyst being deployed in a solar-driven photoelectrochemical (PEC) cell for H_2 evolution in Figure 3F.[58] The cell consisted of a $MAPbI_3-TiO_2$ nanorod array (TNA) as the photoanode, achieving efficient and stable H_2 evolution in HI solution (57 wt % HI aqueous solution saturated with $MAPbI_3$ powder). The amount of evolved H_2 on different PEC cells at 0.14 V vs Ag/AgCl is shown in Figure 3G, in comparison to $MAPbI_3$/c-TiO_2/FTO and $MAPbI_3$/TNA/FTO, the $MAPbI_3$/TNA/c-TiO_2/FTO PEC cell exhibits the highest hydrogen evolution rate of 33.3 $\mu mol/cm^2/h$ under solar illumination, and this during 5 h of experiment.

Because of the precipitation−solubility equilibrium, MHPs remain stable in the saturated HX acid solution, and additionally it can circumvent PbX_2 precipitation and suppresses the formation of the hydrated MHP phase.

As summarized in Table 1, these promising examples demonstrate that saturated aqueous halogen acid solutions offer a suitable reaction medium for MHP-based photocatalytic hydrogen evolution. Because of the precipitation−solubility equilibrium, MHPs remain stable in the saturated HX acid solution, and additionally it can circumvent PbX_2 precipitation and suppresses the formation of the hydrated MHP phase. Analogous to the approach taken within the field of photovoltaic solar cells, introducing heterogeneous interfaces (or even compositional grading within the MHP) can tune the energetics of the photocatalyst system for greatly improved charge separation and reaction activity. However, within the HX acid solution, X^- acts as a sacrificial agent and the oxidation of X^- to X_3^- takes priority over H_2O oxidation. Thus, additional reducing agents such as H_3PO_2 need to be consumed to reduce X_3^- back to X^-, however, this ultimately limits the added value of this reaction.[103] Furthermore, the strong acidity of HX will prevent the selection of certain cocatalysts which are unstable in such environments.

Under such environmental conditions, the relatively weak dipole moment of the solvent does not readily coordinate with the MHP crystal to dissociate them into complexes of the composing ionic species.

Low-Polarity Solvents for CO_2 Reduction. The ionic nature of MHPs makes them especially sensitive to degradation by polar molecules; hence, low-polarity solvents can be employed to create stable photocatalytic reaction conditions. Under such environmental conditions, the relatively weak dipole moment of the solvent does not readily coordinate with the MHP crystal, to dissociate them into complexes of the composing ionic species. This strategy was utilized by both Kuang et al.[62] and Sun et al.,[71] employing all-inorganic $CsPbBr_3$ quantum dots (QDs) for photocatalytic CO_2 reduction; note that due in contrast to the micrometer-sized crystals utilized in haloacids this approach also works for MHP nanocrystals and QDs. In Sun's paper, the low-polarity solvent used was ethyl acetate mixed with trace amounts of water as hole scavengers (volume ratio: 300:1) (see Figure 4A).[71] Within 8 h of simulated solar light irradiation, 34, 12, and 0.8 μmol/g of CO, CH_4, and H_2, respectively, were generated; note that water acts as hole scavenger thus generating oxygen, but also water splitting into hydrogen is competing with the CO_2 reduction reaction. The reaction processes can be summarized as eqs 5−8:

$$2H_2O \rightarrow O_2 + 4H^- + 4e^- \tag{5}$$

$$2H^+ + 2e^- \rightarrow H_2 \tag{6}$$

$$CO_2 + 2e^- + 2H^+ \rightarrow CO + H_2O \tag{7}$$

$$CO_2 + 8e^- + 8H^+ \rightarrow CH_4 + 2H_2O \tag{8}$$

The $CsPbBr_3$ QDs displayed a good structural stability under these conditions and maintained the surface morphology and crystalline structure during the reaction.[71] In Kuang's work, with 12 h of constant illumination, 49.5, 22.9, and 1.07 μmol/g of CO, CH_4, and H_2 are produced on the $CsPbBr_3$ QDs.[59] To further boost the performance, as depicted in Figure 4B, the $CsPbBr_3$ QDs were modified by the addition of graphene oxide (GO) which is capable of efficient electron extraction and transport.[62] The generated $CsPbBr_3$/GO composite had a ca. 25% enhanced electron consumption rated (357.4 μmol/g) in comparison to pristine $CsPbBr_3$ material (284.7 μmol/g) as is shown in Figure 4C. In this latter example, pure ethyl acetate without addition of water was used as the reaction medium. The nature of the hole scavenger in this system is unclear.

This concept was expanded in the work of Xu et al., where $CsPbBr_3$ QDs/graphitic carbon nitride (g-C_3N_4) composites were engineered for efficient CO_2 photoreduction. It was found that the presence of g-C_3N_4 improves the electron extraction via type-II bandgap alignment and the chemical bond formed

Table 1. Summary of Reported Photocatalytic Hydrogen Generation Activity from Haloacid (HX) Solution Using MHP-Based Systems

photocatalyst	solution	light source	activity (μmol/g/h)	measured time for stability (h)	ref
$MAPbI_3$	HI solution	visible light ($\lambda \geq 475$ nm)	33	160	28
Pt/TiO_2-$MAPbI_3$	HI solution	visible light ($\lambda \geq 420$ nm), 200 mW/cm^2	7300	12	57
$MAPbI_3$/rGO	HI solution	visible light ($\lambda \geq 420$ nm), 300 W	939	200	53
$Cs_2AgBiBr_6$	HBr solution	visible light ($\lambda \geq 420$ nm), 300 W	48.9	120	61
Black Phosphorus/$MAPbI_3$	HI solution	visible light ($\lambda \geq 420$ nm), 300 mW/cm^2	3472	200	59
PEDOT:PSS/$MAPbBr_3$/Ta_2O_5	HBr solution	visible light ($\lambda \geq 420$ nm), 150 mW/cm^2	650	4	56
$MAPbBr_{3-x}I_x$/Pt	HBr/HI mix solution	visible light ($\lambda \geq 420$ nm), 300 W	2604.8	50	54
$CsPbBr_{3-x}I_x$/Pt	HBr/HI mix solution	visible light ($\lambda \geq 420$ nm), 300 W	1120	50	55
$MA_3Bi_2I_9$/Pt	HI solution	visible light ($\lambda \geq 400$ nm), 300 W	170	70	60

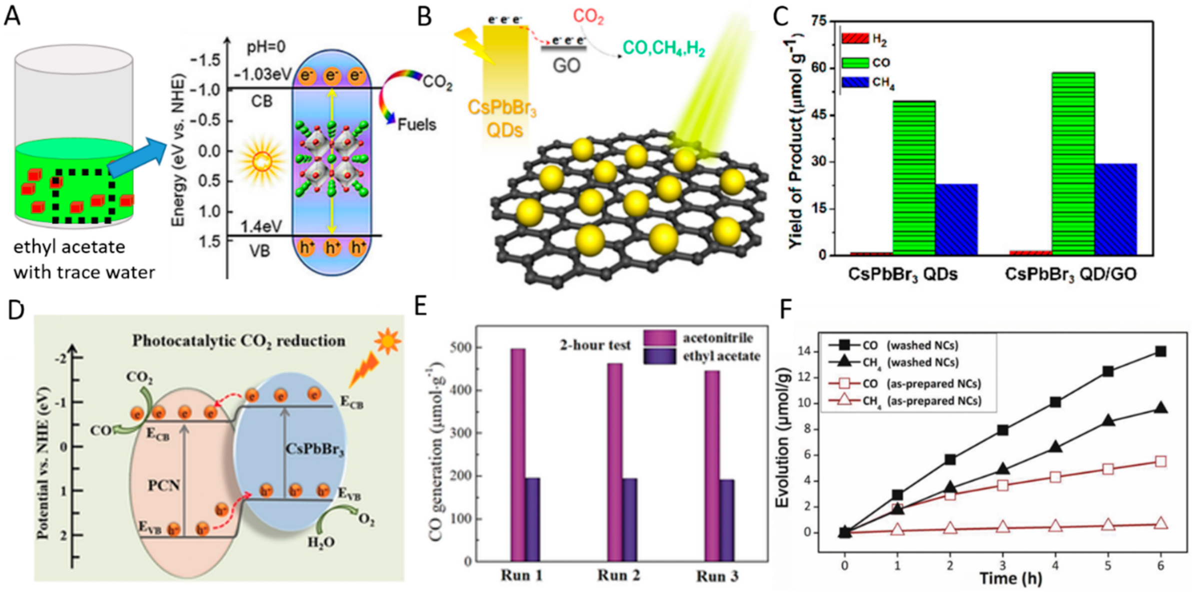

Figure 4. (A) $CsPbBr_3$ for the photocatalytic CO_2 reduction in a 300/1 ethyl acetate/water mixture. Reproduced with permission from ref 71. Copyright 2017 John Wiley and Sons. (B) Scheme of the $CsPbBr_3$ with graphene oxide for photocatalysis CO_2 reduction in ethyl acetate and (C) the yield of products in this reaction system.[62] Reproduced from ref 62. Copyright 2017 American Chemical Society. (D) Band alignment of the composite photocatalyst $CsPbBr_3$ QDs/g-C_3N_4 for photocatalysis CO_2 reduction in acetonitrile and ethyl acetate and (E) the CO generation for three consecutive runs of 2 h each in acetonitrile/water and ethyl acetate/water system on this composite.[69] Reproduced with permission from ref 69. Copyright 2018 John Wiley and Sons. (F) Time course of CO and CH_4 evolutions via CO_2 reduction by $Cs_2AgBiBr_6$ NCs in ethyl acetate.[72] Reproduced with permission from ref 72. Copyright 2018 John Wiley and Sons.

between MHPs and g-C_3N_4, as shown in Figure 4D. In this work, both acetonitrile and ethyl acetate solvents with trace amounts of water (volume ratio: 300:1) were employed, yielding CO with the formation rates of 148.9 and 70 μmol/g/h, respectively.[69] Furthermore, Figure 4E presents that with 3 successive cycles of catalysis (6 h in total), only 10.3% and 2.4% activity was lost in the acetonitrile/water and ethyl acetate/water systems, respectively. The enhanced stability can be attributed to the surface passivation of $CsPbBr_3$ by g-C_3N_4, through the interaction between the amino group on the edges of heptazine in g-C_3N_4 and Br^- in $CsPbBr_3$ QDs. Building on this work, Zhang et al. coupled $CsPbBr_3$ to g-C_3N_4 containing titanium-oxide species, to prepare $CsPbBr_3$/TiO-g-C_3N_4, which exhibits improved activity on CO_2 reduction in an ethyl acetate/water system, in comparison to $CsPbBr_3$/g-C_3N_4. Here titanium-oxide species helped to speed up the charge separation and acted as reaction sites to improve the surface reaction.[75] In a similar fashion, the good charge conductivity of two-dimensional layered $Ti_3C_2T_x$ (T_x: fluorine, oxygen, and hydroxyl groups) MXene material was exploited by Liu et al. to accelerate the photogenerated charge separation in $CsPbBr_3$ nanoparticles. The MXene-MHP photocatalyst yielded CO and CH_4 production rates of 32.15 and 14.64 μmol/g/h, respectively, in pure ethyl acetate solution.[73]

Partial bromide substitution by chloride in $CsPbBr_3$ to form $CsPbBr_{3-x}Cl_x$ QDs was used by Su et al. to generate MHPs with improved stability for the CO_2 reduction.[70] However, the increased Cl content reduces the visible light response. This shows the need for finding a balance between stability and activity/photoresponse within a chosen MHP photocatalyst through well-informed materials engineering.

Moving away from Pb-based MHPs to lead-free perovskites, Kuang et al. showed CO_2 reduction over $Cs_2AgBiBr_6$ NCs under solar illumination in pure ethyl acetate.[72] The stable evolution of CO and CH_4 on $Cs_2AgBiBr_6$ NCs under simulated solar light irradiation is shown in Figure 4F. After 6 h of irradiation, 5.5 and 0.65 μmol/g of CO and CH_4 are generated on $Cs_2AgBiBr_6$, respectively, with no H_2 side product detected.

CO_2 reduction in low-polarity solvents with or without trace amounts of water as electron donor expands the potential

Table 2. Summary of the Reported Photocatalytic CO_2 Reduction Performance of MHPs under Various Illumination Conditions

photocatalyst	solution	light source	products and activities (μmol/g/h)	measured time for stability (h)	ref
$CsPbBr_3$ QDs	ethyl acetate/water	300 W Xe lamp, AM 1.5G filter	CO(4.25), CH_4(1.5), H_2(0.1)	8	71
$CsPbBr_3$QDs/GO	ethyl acetate	300 W Xe lamp, AM 1.5G filter, 150 mW/cm^2	CO(4.89), CH_4(2.47), H_2 (0.13)	12	62
$CsPbBr_3$QDs/g-C_3N_4	ethyl acetate/water	300 W Xe lamp 420 nm cutoff filter	CO(70)	6	69
	acetonitrile/water		CO(148.9)		
$CsPbBr_3$/TiO-g-C_3N_4	ethyl acetate/water	300 W Xe lamp, 400 nm cutoff filter, 100 mW/cm^2	CO(12.9)	10	75
$CsPbBr_3$/MXene	ethyl acetate	300 W Xe lamp 420 nm cutoff filter	CO(32.15), CH_4 (14.64)	12	73
$CsPbBr_{3-x}Cl_x$ QDs	ethyl acetate	300 W Xe lamp, AM 1.5 filter, 200 mW/cm^2	CO(85), CH_4 (12)	8	70
$Cs_2AgBiBr_6$	ethyl acetate	300 W Xe lamp, AM 1.5G filter, 150 mW/cm^2	CO(0.92), CH_4 (0.11)	6	72
$CsPbBr_3$@TiO_2	ethyl acetate/isopropanol	300 W Xe lamp, AM 1.5G filter, 150 mW/cm^2	CO(3.9), CH_4 (6.72), H_2 (1.46)	30	81
$MAPbI_3$@Fe-MOF	ethyl acetate/water	300 W Xe lamp, 400 nm cutoff filter, 100 mW/cm^2	CO(4.16), CH_4 (13)	80	83
$Co_{2\%}$@$CsPbBr_3$/Cs_4PbBr_6	water	300 W Xe lamp, 400 nm cutoff filter, 100 mW/cm^2	CO(11.95)	20	92
$CsPbBr_3$@ZIF-67	water vapor	100 W Xe lamp, AM 1.5G filter, 150 mW/cm^2	CO(0.77), CH_4 (3.51)	18	84
$CsPbBr_3$NC/ZnO nanowire/macroporous graphene	water vapor	A 150 W Xe lamp, AM 1.5G and 420 nm cutoff filter, 150 mW/cm^2	CO(0.85), CH_4 (6.29)	16	96
Cs_2SnI_6/SnS_2	water and methanol vapor	150 mW/cm^2 visible light, 400 nm long pass filter	CH_4 (6.09)	9	97
$Cs_3Bi_2I_9$	water vapor	UV lamp, 80.38 μW/cm^2	CO(7.76), CH_4 (1.49)	10	98

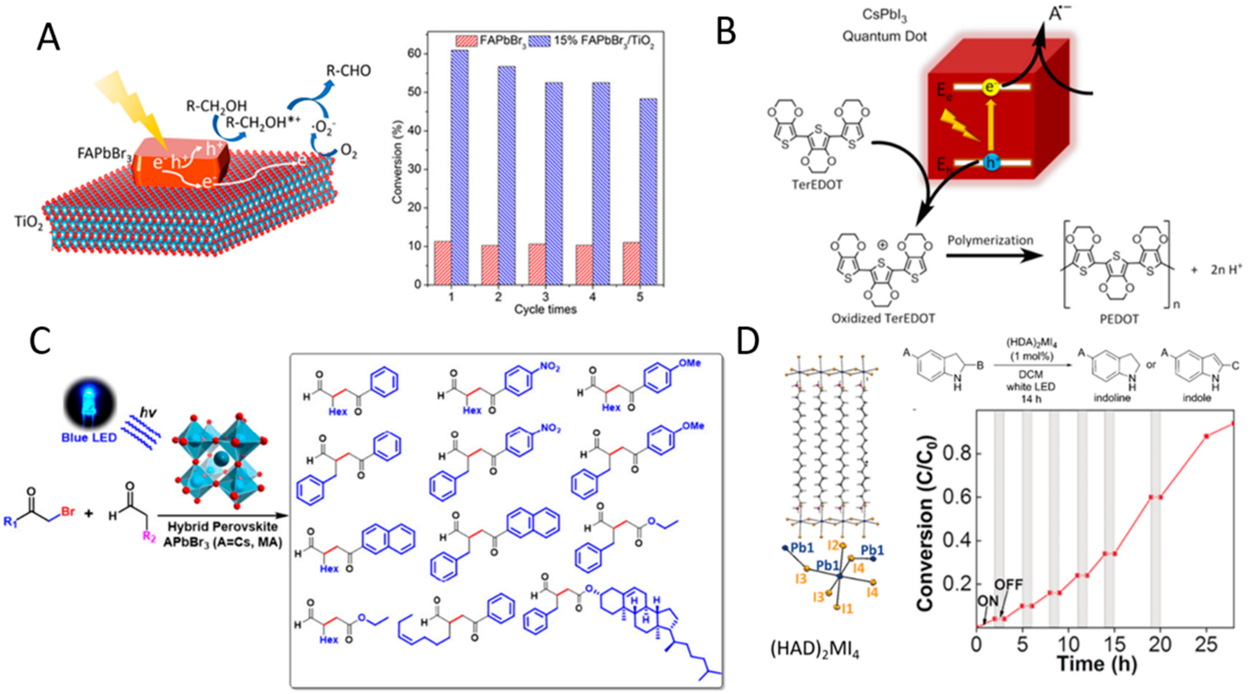

Figure 5. (A) Schematic of the $FAPbBr_3/TiO_2$ using for photocatalytic benzyl alcohol oxidation, and recycle test of photocatalytic oxidation of benzyl alcohol over pure $FAPbBr_3$ and 15%$FAPbBr_3/TiO_2$ hybrids.[63] Reproduced from ref 63. Copyright 2018 American Chemical Society. (B) Photocatalytic polymerization of TerEDOT by $CsPbI_3$ QDs under visible light illumination.[67] Reproduced from ref 67. Copyright 2017 American Chemical Society. (C) Photocatalytic α-alkylation of aldehydes by Cs/$MAPbBr_3$ in organic solvents.[66] Reproduced from ref 66. Copyright 2019 American Chemical Society. (D) Crystal structures and photocatalytic activity of 2D $(HDA)_2MI_4$(M = Pb, Sn) for indoline-2-carboxylic acid decarboxylation in 25 h.[80] Reproduced with permission from ref 80. Copyright 2019 John Wiley and Sons.

application of MHP photocatalysts, as summarized in Table 2. In most reports, MHPs still face a poor product selectivity as CO and CH_4 are typically generated simultaneously, and additionally water splitting generating H_2 is competing for the generated photoelectrons while the holes are scavenged by water forming O_2. Nonetheless, employing a largely apolar environment, even with the inclusion of trace amounts of targeted polar molecules, is a promising route toward long-term activity and stability.

Low-Polarity Solvents for Organic Transformations. Next to the photoreduction of CO_2 for the generation of solar fuels, recent efforts have focused on organic transformations within low-polarity solvents for solar-driven MHPs photocatalysis. Roeffaers et al.[63] reported the use of MHPs as photocatalysts for benzylic alcohols oxidation in a nonpolar toluene solution, as shown in Figure 5A. In this study, pure $FAPbBr_3$ microparticles and nanoparticles were proven to be efficient photocatalysts under solar excitation; within 8 h of irradiation, $FAPbBr_3$ microparticles exhibited a conversion rate of roughly 15% with near 100% selectively (0.1 mmol of benzyl alcohol in 2.5 mL of toluene, 10 mg of catalyst). More importantly, after 5 reaction cycles (40 h in total) the $FAPbBr_3$ photocatalyst displayed no decrease in activity. Again, the activity of the MHP photocatalyst can be improved by selecting a suitable cocatalyst and re-engineering the band structure of the system. For instance, modifying $FAPbBr_3$ into a $FAPbBr_3/TiO_2$ hybrid nanomaterial by *in situ* antisolvent growth realized the highest conversion rate of benzyl alcohol when optimized (ca. 63% conversion, with 15 wt % $FAPbBr_3$ in $FAPbBr_3/TiO_2$ composite), being 4 times greater than the pristine MHP case. However, after TiO_2 was incorporated, the increased activity comes at the cost of compromising the stability of the photocatalyst, which is mainly attributable to a breakdown of $FAPbBr_3$ following aldehyde and water generation. Similar results were obtained by Tüysüz et al., where they have prepared $CsPbBr_3/TiO_2$ for benzylic alcohol oxidation in toluene.[79]

Also other organic transformations have been explored on MHP photocatalysts. For instance, as shown in Figure 5B, Tüysüz et al. found that $CsPbI_3$ QDs can promote the polymerization of 2,2′,5′,2″-ter-3,4-ethylenedioxythiophene (TerEDOT) to poly(3,4-ethylenedioxythiophene) (PEDOT) in dry toluene under visible light illumination.[67] In fact, the generated PEDOT further stabilizes the cubic perovskite phase of $CsPbI_3$ QDs by encapsulating the perovskites and shielding it from the environment. The direct functionalization of saturated C−H bonds to form high value-added chemicals is another challenging topic in modern chemistry. Roeffaers et al. recently used $FAPbBr_3$ bulk microcrystals to photoactivate the $C(sp^3)$-H bond in aromatic hydrocarbons and to form the corresponding alcohols and aldehydes.[64] Similar to tailoring the energetics within solar cells, the addition of an electron-transfer layer (TiO_2) and hole-transfer layer (NiO_x) allowed for optimizing the conversion efficiency of the MHP photocatalyst, by improving charge separation properties. This $TiO_2/FAPbBr_3/NiO_x$ system achieved $C(sp^3)$-H bond activation in toluene with high selectivity and high conversion rates of benzaldehyde generation from toluene (3800 μmol/g/h).[64] Very recently, Tüysüz et al. confined $Cs_3Bi_2Br_9$ nanoparticles (2−5 nm) inside large ordered channels of mesoporous silica SAB-15 and used this composite for aliphatic and aromatic C−H bond activation, to develop corresponding aldehydes and ketones.[78] This study demonstrates that well-dispersed MHP nanoparticles offer a better electron−hole separation and an improved contact with reaction substrates.

Besides the selective oxidation of organics to value-added products in toluene, the complete mineralization of organics to CO_2 and H_2O using MHP photocatalysts has also been investigated. Huang et al. synthesized $CsPb(Br_{1-x}Cl_x)_3$-Au NCs for the Sudan Red III degradation in toluene.[76] When the $CsPb(Br_{1-x}Cl_x)_3$-Au NCs system is photoexcited, there is an inner electron field between Au and the perovskite enhancing the charge separation. The dissolved O_2 can be trapped by the photoelectrons on $CsPb(Br_{1-x}Cl_x)_3$ to produce superoxide anion radicals ($^{\bullet}O_2^-$), and Au NCs can act as hole reservoirs to enhance hydroxyl radical generation on its surface.[76] After that, Sudan Red III reacts with these two kinds of radicals to generate nontoxic products. Upon visible light irradiation, 71% Sudan Red III was degraded by $CsPb(Br_{1-x}Cl_x)_3$-Au within 6 h, which is 3 times higher than the $CsPb(Br_{1-x}Cl_x)_3$ case (ca. 20% of Sudan Red III degradation). Here, the role of Au NCs is in contrast to the widely employed nonplasma Au-nanoparticle decorated photocatalysts,[104,105] where Au extracts electrons from the semiconductors and acts both as an electron reservoir and a reduction site.

Beyond photocatalytic organic transformations in toluene, other low-polarity solvents like dichloromethane (DCM), tetrahydrofuran (THF), dioxane, and hexane have been used for MHP-based photocatalytic organic transformations. Wu et al.[68] achieved S−H bond activation using $CsPbX_3$ (where X = Cl, Br, and I) NCs in DCM. Interestingly, this work also realized C−H activation by evaluating phosphorylation of N-aryl tetrahydroisoquinoline derivatives in both toluene and THF solvent. As seen in Figure 5C, Yan et al. demonstrated that $MAPbBr_3$ and $CsPbBr_3$ nanocrystals could selectively form C−C bond in α-alkylation of aldehydes in DCM, THF, and dioxane, via photocatalysis.[66] A large turnover number (TON) of over 52 000 is achieved in the perovskite-based photocatalytic α-alkylation of aldehydes, under visible light illumination. This large TON is encouraging for this particular application and can potentially provide a path toward the commercialization of perovskite photocatalysis in the future. Follow up work by Yan and co-workers showed that not only C−C bond formation but also a series of organic transformation, C−O and C−N bond-formation, can be achieved on the $CsPbBr_3$ photocatalyst.[65] In ethyl acetate, $CsPbBr_3$ can achieve C−N bond formations via direct N-heterocyclizations forming pyrazoles and pyrroles, upon irradiating with blue light. With a Ni cocatalyst, C−O bond formation via aryl-esterification was realized on $CsPbBr_3$ in THF, upon irradiating with blue light. In addition, $CsPbBr_3$QDs can drive the MBT (2-mercaptobenzothiazole) oxidation in hexane by photocatalysis and photoelectrocatalysis.[74] Recently, Gualdrón-Reyes and co-workers prepared $CsPbBr_3/I_{3-x}$ nanoparticles via both hot injection (H-I-$CsPbBr_3/I_{3-x}$) and anion exchange (A-E-$CsPbBr_3/I_{3-x}$) methods, to investigate the influential role of the surface chemical states in the photo-oxidation of β-naphthol in hexane.[77] The two different preparation methods arrived at $CsPbBr_3/I_{3-x}$ nanoparticles with different iodide vacancy (V_I) concentrations on the surface, with a larger V_I population found in A-E-$CsPbBr_3/I_{3-x}$. As a result, A-E-$CsPbBr_3/I_{3-x}$ formed superoxide radicals, $^{\bullet}O_2^-$, species involved in the photodegradation of organic compounds. The V_I sites were found to provide key surface chemical states to produce $^{\bullet}O_2^-$. On the other hand, the VB is shifted to more negative values and the bandgap is narrowed in H-I-$CsPbBr_3/I_{3-x}$ by increasing the iodide content.

As shown in Figure 5D, Soo et al. synthesized 2D Pb and Sn halide perovskite microcrystals with the long-chain alkyl group 1-hexadecylammonium (HDA): $(HDA)_2PbI_4$ and $(HDA)_2SnI_4$.[80] These MHPs exhibited photocatalytic activity in decarboxylation and dehydrogenation of indoline-2-carboxylic acids in DCM. Figure 5D presents the stable performance of these materials during a 25 h "on−off" irradiation study. However, if the two Pb- and Sn-based perovskites are compared, the Sn-based structures exhibit inferior stability due to the self-oxidation of Sn^{2+} to Sn^{4+}.

This collection of recently reported results using MHPs as photocatalyst in low-polarity solvents demonstrates their potential in a wide range of photocatalytic reactions, including CO_2 reduction, selective organic transformations for value-added products, and organic pollutant degradation. The reduced polarity of the created environment results in a relatively low solubility for MHPs which preserves the original structure rather than relying on a precipitation−solubility equilibrium as was discussed for aqueous conditions. Under these conditions, MHP nanoparticles and QDs can be used to drive photocatalytic reactions rather than micrometer-sized MHPs in water, further optimizing the accessible surface area.

> A straightforward stabilization method consists of encapsulating the MHP by a protective layer inside core−shell particles.

Encapsulation. A straightforward stabilization method consists of encapsulating the MHP by a protective layer inside core−shell particles. The protective layer prevents direct contact between the MHP and destabilizing polar molecules. Care should be taken that the shell material does not block the light from reaching the MHP. Kuang and co-workers used amorphous TiO_2 as the encapsulating material to generate $CsPbBr_3@TiO_2$ core−shell structures.[81] Figure 6A shows the TEM picture of this core−shell structure in which the $CsPbBr_3$ nanocrystal was capped by amorphous TiO_2. This photocatalyst was used for CO_2 reduction in ethyl acetate/water under solar light irradiation, exhibiting better activity than bare $CsPbBr_3$ because of improved electron transfer from $CsPbBr_3$ to TiO_2. Most importantly, this core−shell structure shows impressive stability improvement, retaining over 90% of its initial photocatalytic activity after 15 h of use. Even after 30 h of constant simulated solar light illumination, the encapsulated material still possessed comparable photocatalytic activity, as shown in Figure 6B. Recently, Wu et al. covered $CsPbBr_3$ microparticles with porous graphitic carbon nitride (p-g-C_3N_4) and used it for malachite green degradation in polar isopropanol. This catalyst exhibited a stable activity during 10 cycles (∼4.7 h in total), as p-g-C_3N_4 acted to protect the $CsPbBr_3$ surface.[94] The core−shell structure was also shown to help stabilize the MHP not only in low-polarity solvents but also in a high-polarity solvent like water.

Zheng et al. also prepared anatase-coated $CsPbBr_3$ nanoparticles for photocatalytic applications; Figure 6C displays a TEM micrograph of the core−shell system.[82] The tight TiO_2 shell was prepared via a two-step process, which starts from a simple wet chemical hydrolysis of titanium butoxide in relative humidity (RH) of 30%, to form a TiO_x layer outside the $CsPbBr_3$ NC at 25 °C. Next, a 300 °C heating step promotes the formation of the tight TiO_2 (a-TiO_2). Compared to pristine $CsPbBr_3$ NCs, the core/shell $CsPbBr_3$/a-TiO_2 NCs present a higher photocurrent and a smaller resistance in 0.1 m Na_2SO_4 aqueous solution due to the formation of type II band alignment in the $CsPbBr_3$/a-TiO_2 core/shell heterostructure. On the other hand, the $CsPbBr_3$/a-TiO_2 composite was relatively stable and was able to be stored in water for more than 12 weeks in the dark without leading to any phase change or chemical decomposition. Furthermore, within 8 h of irradiation, as shown in Figure 6D, the photocurrent of core/shell NCs does not show any reduction, indicating excellent PEC stability in water. A protective layer on the outside of MHPs, especially a tight crystallized shell, could decrease the direct contact from the polar solvent which indeed enhances the stability of the MHP photocatalyst.

On the other hand, encapsulation is not merely limited to the synthesis of individual core−shell photocatalyst structures, as shown in Figure 6A,C. The small size of MHP QDs allows trapping porous structures such as metal−organic frameworks (MOFs). $CsPbBr_3$ QDs trapped in the ZIF-type MOFs (ZIF-67, ZIF-8) showed a steady CO_2 photoreduction in an ethyl acetate and water mixture.[84] Figure 6E presents a schematic of the synthesized $CsPbBr_3@ZIF$ hybrids by directly growing ZIF around $CsPbBr_3$ QDs. The catalytic stability of $CsPbBr_3@ZIF$ was also tested by a recycling photocatalytic reaction. After cycling 6 times (18 h in total), no obvious decay was obtained in Figure 6F, indicating the good protective function of the ZIF shell. Very recently, Lu et al. incorporated iodide-based perovskite $MAPbI_3$ into Fe-MOF, which exhibited an impressive activity on CO_2 reduction in an ethyl acetate/water solution (over 80 h: CO, 4.16 μmol/g/h; CH_4, 13 μmol/g/h).[83] Ghosh et al. incorporated a Br-based perovskite into the ZIF-8 pore structure to prepare a composite photocatalyst, MA(OA)-$PbBr_3@ZIF$-8 (OA is n-octylammonium).[86] OA, a long alkyl chain ammonium cation, was used as a capping ligand to stabilize the MHP nanoparticles and control the crystallization process for the formation of colloidal NPs inside the MOF.[86] This material presents outstanding chemical stability under a variety of conditions which would normally be detrimental for the MHPs, such as water immersion, UV light irradiation, and high-temperature (100 and 140 °C) heating. Furthermore, they exhibit promising activity and stability toward photocatalytic organic dye (methyl orange) degradation in water.[86] Although the photogenerated holes found in the VB of MA(OA)$PbBr_3$ cannot directly oxidize H_2O, the electrons in the CB will react with O_2 to generate superoxide radicals ($^{\bullet}O_2^-$) which react with H_2O to produce the hydroxyl radicals.

Alternatively, adding hydrophobic ligands to coat the NC surface is another effective method toward creating a waterproof "shell" on the MHP crystal exterior. Lu et al. adopted this approach with their $CsPbBr_3/Cs_4PbBr_6$ nanocrystals and used the highly hydrophobic ligand hexafluorobutyl methacrylate.[92] The resultant MHP-based system possessed an outstanding tolerance to H_2O; after 100 h of storage in water, 90% of the PL intensity of this MHP component was retained. Further doping the photocatalyst with Co (generating $Co_{2\%}@CsPbBr_3/Cs_4PbBr_6$) allowed for a CO yield of roughly 240 μmol/g in 20 h via CO_2 reduction, in pure water. Similarly, larger hydrophobic organic spacer cations (A-site cation, such as 2-phenylethylammonium (PEA) or *n*-butylammonium (n-BA)) have been used to form lower-dimensional 2D or quasi-2D layer perovskites.[106] The addition of these A-site cations has been found to benefit the overall material stability in polar environments, by acting as a protecting layer against moisture attack. These improvements to stability have been widely demonstrated for MHP-based solar cells and LEDs and offer a promising direction toward developing more stable MHP photocatalysts in the future.

Coating MHPs with hole and electron transport layers (HTL and ETL, respectively) and electrodes in PEC devices also prevents direct contact with polar solvents, providing another effective route toward long-term stabilization. Currently, there are two different directions for this particular approach: (1) implementing an MHP solar cell−electrode (photoelectrode) system, with the MHP PV separated completely from the electrode and electrolyte; (2) MHP photoelectrode, with the

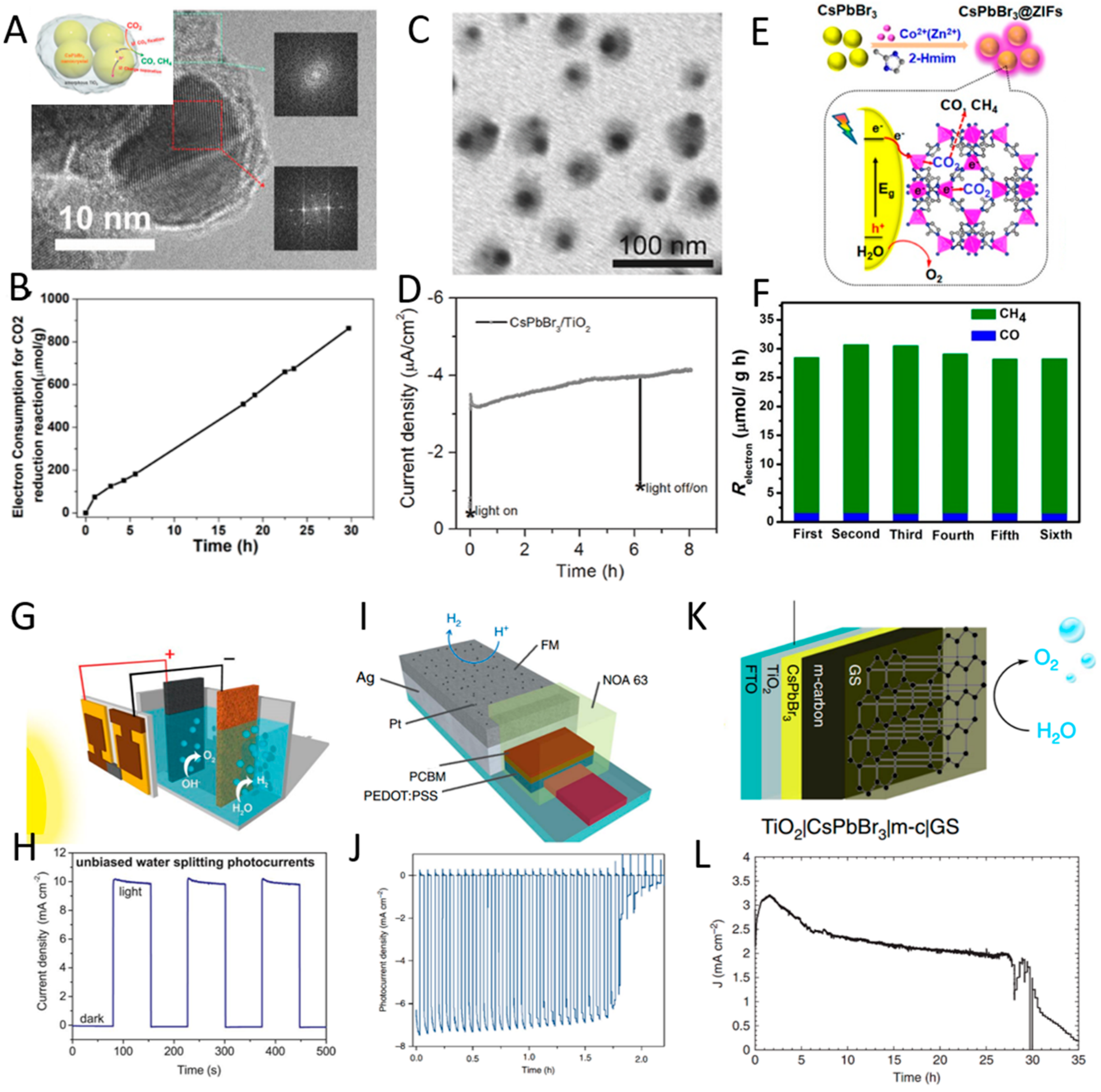

Figure 6. (A) TEM images of amorphous TiO_2-encapsulated $CsPbBr_3$ nanocrystal and (B) time course of photocatalytic CO_2 reduction in ethyl acetate with isopropanol traces upon solar light irradiation.[81] Reproduced with permission from ref 81. Copyright 2018 John Wiley and Sons. (C) TEM image of anatase TiO_2-coated $CsPbBr_3/TiO_2$ core/shell NCs and (D) controlled potential electrolysis of the $CsPbBr_3/TiO_2$ NCs electrode in neutral water within 8 h.[82] Reproduced with permission from ref 82. Copyright 2018 John Wiley and Sons. (E) Schematic of $CsPbBr_3$@ZIF-67 formation and the charge transfer in this material and (F) its application for CO_2 photoreduction in ethyl acetate solution.[84] Reproduced from ref 84. Copyright 2018 American Chemical Society. (G) Perovskite water-splitting solar cell and (H) current density−time curve of the device without external bias under solar light illumination.[90] Reproduced with permission from ref 90. Copyright 2014 The American Association for the Advancement of Science. (I) Structure diagram of FTO/PEDOT:PSS/perovskite/PCBM/PEIE:Ag photocathode for water reduction and (J) the photocathode stability test by light-chopped chronoamperometry.[91] Reproduced with permission from ref 91. Copyright 2016 Springer Nature. (K) Schematic diagram of $TiO_2|CsPbBr_3|$m-c|GS photoanode and (L) its long-term stability of $TiO_2|CsPbBr_3|$m-c|GS70 for water oxidation with solar light irradiation.[94] Reproduced with permission from ref 94. Copyright 2019 Springer Nature.

MHP integrated into the electrode. Grätzel and co-workers were the first to construct an MHP-based solar cell-electrode (photoelectrode) system, for the application of water splitting in an alkaline electrolyte. Here, they combined a perovskite tandem solar cell and a bifunctional NiFe layered double hydroxide (i.e., origin of both water oxidation and reduction), with the perovskite placed out of the solution to keep it stable, as shown in Figure 6G.[90] Under solar light irradiation, this device offered relatively impressive water-splitting performance; Figure 6H shows the "on−off" current density−time curve of the device without external bias for water splitting in which the unbiased water splitting current reached 10 mA/cm^2, which corresponds to a 12.3% solar-to-hydrogen efficiency. Kamat et al. and Mathews et al. proposed MHP-based solar cell ensembles with $BiVO_4$ and Fe_2O_3 photoanodes, respectively, for the same water-splitting reactions.[87,89] Using these photoanodes, a single-junction $MAPbI_3$ solar cell can achieve water splitting, as holes in these photoanodes can mediate water oxidation. Specifically, the $BiVO_4$-$MAPbI_3$ and Fe_2O_3-$MAPbI_3$ exhibited solar-to-hydrogen conversion efficiencies of 2.5% and 2.4% at neutral pH, respectively.

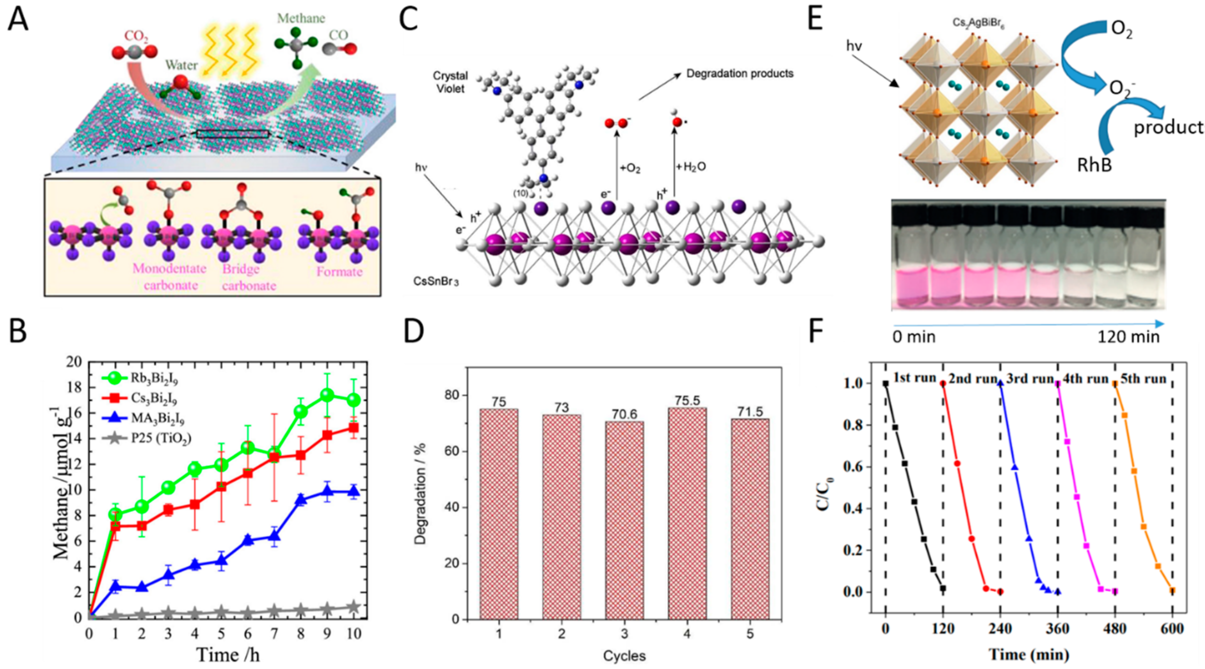

Figure 7. (A) Scheme of CO_2 photoreduction with water vapor on Bi-based perovskite photocatalysts and (B) the CH_4 generation for 10 h.[98] Reproduced from ref 98. Copyright 2019 American Chemical Society. (C) Scheme of the photodegradation crystal violet on the $CsSnBr_3$ and (D) stability test for the photodegradation of crystal violet in 5 cycles.[99] Reproduced with permission from ref 99. Copyright 2018 John Wiley and Sons. (E) Scheme of the photodegradation of RhB on the $Cs_2AgBiBr_6$ and photographs of RhB at different irradiation times and (F) recycling test of photocatalytic RhB degradation upon visible-light irradiation.[100] Reproduced with permission from ref 100. Copyright 2019 John Wiley and Sons.

Meanwhile, some researchers appropriately integrated MHPs into the electrode to prepare an MHP photoelectrode for the PEC reaction. In 2015, Zheng et al. reported the first $MAPbI_3$-photoelectrode for water splitting.[88] In this work, a Ni layer was coated onto $MAPbI_3$ both as a physical passivation barrier and as a hole transport layer. However, after 15−20 min of continuous tests, the photocurrent of this photoelectrode experienced a sharp decrease. Reisner et al. further adopted a solar cell-like structure to develop a metal-encapsulated perovskite photocathode, FTO/PEDOT:PSS/$MAPbI_3$/PCBM([6,6]-phenyl-C_{61}-butyric acid methyl ester)/PEIE(ethoxylated polyethylenimine):Ag, for PEC hydrogen evolution in an aqueous medium.[91] As shown in Figure 6I, the perovskite solar cell provides the photocathode and two additional protective layers, composed of Ag and an eutectic alloy (InBiSn), were deposited to fully cover the solar cell. These two protective layers not only form a water-resistant metal-encapsulated photocathode and protect the perovskite but also transfer the photogenerated electrons to the surface to react with water. This photocathode can be stored in water for 6 h without any decomposition. Furthermore, as shown in Figure 6J, the photocathode retained more than 80% of the initial photocurrent after continuous illumination for 1.5 h. Recently, Poli et al. used graphite sheets (GSs) as a protective layer to create a TiO_2/$CsPbBr_3$/carbon/GS photoanode, as shown in Figure 6K. A 25 μm thick deposit of GS offers a more compact seal to stop water from reaching the perovskite. Furthermore, the GS is superhydrophobic, which also enhances the water-resistance of this photoanode. Under solar illumination, the system remained stable for 30 h in the aqueous electrolyte with above 2 mA/cm^2 photocurrent at 1.23 V_{RHE}.[94]

In 2019, Reisner et al. expanded the reaction scope when using MHP-photoelectrodes for CO_2 reduction. They integrated an MHP-photoelectrode with $BiVO_4$ photoanode to prepare a tandem device for syngas production.[93] Under bias-free operation, this tandem device, which consists of $BiVO_4$, $FAMA_{0.22}Cs_{0.07}Pb_{1.32}I_{3.27}Br_{0.66}$, and cobalt catalyst on carbon nanotubes (CoMTPP@CNT), offers the production rates of H_2 and CO of 0.58 ± 0.33 and 0.18 ± 0.16 μmol/cm^2/h in CO_2 saturated water, respectively. In this tandem device, $FAMA_{0.22}Cs_{0.07}Pb_{1.32}I_{3.27}Br_{0.66}$ and $BiVO_4$ harvest solar light to generate carriers, with holes remaining in the $BiVO_4$ for water oxidation and electrons moving to CoMTPP@CNT for CO_2 and H_2O reduction. The selectivity of products on CoMTPP@CNT can be controlled by the pH of the electrolyte. More H_2 was found to be released in acidic solutions; relatively low production was observed in alkaline conditions, and neutral pH favored more CO_2 reduction. Furthermore, in comparison to a single-component photocatalyst, such as a $MAPbBr_3$, a mixed compound $FAMA_{0.22}Cs_{0.07}Pb_{1.32}I_{3.27}Br_{0.66}$ system presents a better efficiency and stability.[107]

Overall, on the basis of the discussion above, MHP film systems achieve "steady" PEC energy conversion in aqueous conditions via several methods, including MHP solar cells coupled with electrocatalyst and photoelectrocatalyst, and protective layers fully covering to form an MHP photoelectrode. In these systems, MHP, as a harvester of light to absorb solar light and generate carriers, was isolated from the aqueous solution. As a result, the stability of MHP would be effectively improved. These PEC systems offer an efficient method for the utilization of solar energy by halide perovskites in aqueous solutions.

Realizing Intrinsic MHP Stability. The approaches outlined above, while offering varying degrees of success under rather regimented conditions, fail to offer a path toward widespread adoption. As has been highlighted throughout, this failure stems from the instability of MHPs when exposed to inherently reactive environments. Clearly, developing MHPs which can intrinsically endure common photocatalytic conditions, and importantly display long-term photocatalytic performance, represents an ideal scenario. In comparison to hybrid organic−inorganic perovskites, all-inorganic perovskites are more stable because of their higher formation energy, lower configurational entropy, nonvolatility, and lower hygroscopic nature.[109] Owing to the elimination of weakly bonded organic components in the crystal structure, all-inorganic perovskites exhibit relatively higher resilience against environmental triggers. Recently, some all-inorganic perovskites have been used with success for reactions employing water vapor. Kuang et al. prepared $CsPbBr_3$ NC/MRGO (macroporous graphene oxide) composite, though they further modified the system by adding hierarchical branched ZnO nanowires (BZNW), generating $CsPbBr_3$/BZNW/MRGO composite, for photocatalytic CO_2 reduction in the presence of water vapor. Compared to both pristine $CsPbBr_3$ NCs and $CsPbBr_3$/MRGO, the addition of the ZnO nanowires enhanced the photoelectron consumption rate to >50 μmol/g/h.[96] Furthermore, during 4 cycles or 16 h of simulated solar illumination, the CH_4 generation remained steady without any apparent decrease. Then, Kuang et al. also explored the stability of lead-free MHP photocatalyst when exposed to polar molecules. With methyl alcohol and water vapor, a lead-free Cs_2SnI_6 perovskite nanocrystal combined with SnS_2 nanosheets achieved the CO_2 to CH_4 (6.09 μmol/g/h) reduction. This hybrid system provided a stable photocatalytic activity over 3 successful reaction cycles (9 h in total).[97] Similarly, Diau et al. prepared $Rb_3Bi_2I_9$, $Cs_3Bi_2I_9$, and $MA_3Bi_2I_9$ with an ultrasonication top-down method, arriving at materials which can remain stable for 7 days under 70% humidity.[98] These perovskites were then used for CO_2 photoreduction with water vapor. As shown in Figure 7A, CO_2 and H_2O can be adsorbed on the perovskite surface and form different intermediate species, including dioxycarbon anion bridge carbonate, monodentate carbonate, and bidentate carbonate. The time-dependent evolution of CH_4 on these perovskites under light irradiation is shown in Figure 7B, in which the production of CH_4 increases steadily for 10 h. More surprisingly, in 2018, Navas et al. prepared $CsSnBr_3$ microparticles for photocatalytic dye degradation in water solution.[99] As the $CsSnBr_3$ VB (1.9 eV vs RHE) is more positive than the redox potential of $OH^-/{}^\bullet OH$,[108] the generated hydroxyl radicals degraded the violet dye as shown in Figure 7C. Meanwhile, as shown in Figure 7D, within 5 cycles (15 h in total) in 2.0 mg/L crystal violet dye aqueous solution, there was no compromise in the photoactivity.

On the other hand, researchers have also explored all-inorganic MHP photocatalysts for steady operation in alcohols. For example, Fan et al. prepared $CsPbBr_3$ nanoparticles for tetracycline hydrochloride (TC-HCl, antibiotic) degradation in ethanol.[102] Upon visible light irradiation, 76% TC-HCl could be degraded in 30 min. Within 4 cycles of experiments for a total of 120 min, $CsPbBr_3$ still maintained nearly 90% of its initial activity. The partial activity loss can be attributed to the loss of photocatalyst material during recovery between consecutive cycles. Relying on the relatively higher chemical robustness of $Cs_2AgBiBr_6$, Xu et al. demonstrated microparticles of this material suitable for photocatalytic reaction in ethanol.[100] In Figure 7E, with continuous irradiation, ca. ∼98% Rhodamine B (RhB) was degraded by $Cs_2AgBiBr_6$ photocatalyst within 2 h. In this reaction, the efficient production of superoxide radicals provides the dominant species involved in RhB degradation. As shown in Figure 7F, the material maintained its photoactivity and comparable stability in ethanol following 6 h of irradiation (5 cycles), although a little bit of AgBr generated as water molecules might lead to partial dissolution of the $Cs_2AgBiBr_6$ crystal. Similarly, Tüysüz et al. synthesized lead-free perovskite $Cs_3Bi_2Br_9$ submicrometer/nanoparticles and used them for the ring-opening reaction of epoxides in isopropanol.[101] In $Cs_3Bi_2Br_9$, Lewis acid Bi sites adsorbed and activated epoxides. Upon light irradiation, holes and electrons generated in $Cs_3Bi_2Br_9$ reacted with alcohols and O_2 to form alcohol anions and superoxide radicals, respectively. Alcohol anions and alcohol radicals generated by the reaction between superoxide radicals and alcohols would serve as nucleophiles to react with activated epoxides and form ether. Upon visible light irradiation, 99% styrene oxide was converted by $Cs_3Bi_2Br_9$ after 6 h of irradiation. Furthermore, with 3 cycles (18 h in total), $Cs_3Bi_2Br_9$ still exhibited a decent activity (retaining 80% of its initial photocatalytic activity).

The high humidity tolerance of all-inorganic MHPs makes them ideal materials for the photocatalytic CO_2 reduction in the presence of high-polarity solvent vapors. Furthermore, the photodegradation of organic pollutants has proved that some all-inorganic MHPs remain stable in high-polarity conditions. These discussed results open opportunities to apply these materials to perform chemical conversions involving polar solvents or molecules, even water splitting without the need of haloacids, biomass reforming, and N_2 reduction.

Summary and Prospects. MHP semiconductors are well-documented to exhibit remarkable optical properties, leading to a wide variety of useful optoelectronic applications (i.e., solar cells, LEDs, photodetectors, etc.). Recently, in light of their interesting photophysics, MHPs were repurposed for photocatalytic reactions and solar-to-chemical energy conversion. However, the intrinsically poor stability of their ionic crystal structure represents a major technical hurdle. The instability of MHPs, and finding ways around it, has imposed the largest limit on the scope of heterogeneous photocatalytic reactions they can be effectively applied to.

In this Review, we have examined the recent progress made in the field of MHP-based photocatalysis, focusing on the instability issues currently holding back progress. To overcome material instabilities, several "stable" MHP-based photocatalytic systems have been designed and realized, including H_2 generation from saturated halo acid solutions, CO_2 reduction and organic synthesis in low-polarity solvents, encapsulation and capping of MHPs for CO_2 reduction and photoelectrochemical water splitting, and CO_2 reduction and dye degradation on all-inorganic MHPs with suitable polar solvents. Prospects to intrinsically improve the crystal stability by designing novel composite perovskites have also been demonstrated. On the basis of the current knowledge and material limitations, several promising paths toward improving both the stability and efficiency of MHP-based photocatalysis can be identified:

1. Improving the long-term catalytic cycling and operational stability of MHPs. While conducting reactions in halo acid and low-polarity solutions has been proven effective for several reactions, such approaches are not universal in nature. To enhance resistance to material degradation pathways, synthesizing core−shell structures (e.g., oxide capping layers) with near-perfect coverage will help to limit contact between the MHPs and any polar solvent. MHP-based solar cells have recently made progress with the instability issues associated with operation under ambient conditions, achieving reliable operation times exceeding more than 1000 h. This was achieved by engineering stable device architectures. Thus, employing top and bottom HTL and ETL materials to fully cover MHPs by spin coating, CVD, or ALD offers a promising method to obtain MHP photocatalysts with long-term stability. Furthermore, HTL and ETL would facilitate charge carrier separation and transportation in MHPs. Increasing the valence charges of the dopant ions (doping of trivalent ions at the B site; e.g. Sb^{3+} in $CsPbI_3$) to increase the interaction between the ions and the crystal frame might give rise to intrinsically more stable perovskite structure without the need for additional functionalization. The partial or full substitution for Pb in MHP with other metals has been widely explored for solar cells, LEDs, and other optoelectronic devices.[110,111] Such compositional modification can enhance the stability of MHP devices and does not necessarily compromise the optoelectronic performance. Further exploration of this strategy for photocatalytic applications is highly promising. Recent advances have shown that the perovskite microstructure can be stabilized under water for more than six months by controlling the lead hydroxide peripheral layer in octahedral perovskite geometry under both acidic and basic media at ambient conditions without any additional capping ligands.[112] These water-stable perovskites can be directly explored for solar water splitting under neutral, acidic, and basic conditions. In brief, there is room for significantly improving the stability and lifetime of MHP-based photocatalysts, in comparison to traditional photocatalysts, such as TiO_2 and perovskite oxides ABO_3 (e.g., $SrTiO_3$, $NaTaO_3$ or $NaNbO_3$).

2. Improving the activity of H_2 generation and CO_2 reduction on MHP-based photocatalysts. To date, the highest photocatalytic H_2 generation is achieved on Pt/TiO_2 (1.97 mol/g/h),[113] and the highest CO_2 reduction rate is realized on $Au_3Cu@SrTiO_3/TiO_2$ (3.77 mmol/g/h (CO), with a side production of hydrocarbon (725.4 μmol/g/h)).[114] However, to date the greatest H_2 generation rate and CO_2 reduction rate achieved for MHPs-based photocatalyst are about 7.3 mmol/g/h and 148.9 μmol/g/h (CO) on $BP/MAPbI_3$[59] and $CsPbBr_3/C_3N_4$,[69] respectively, as shown in Tables 1 and 2. There are several clear ways to further enhance the activity of MHPs photocatalysis for H_2 generation and CO_2 reduction: Cocatalysts (Pt, Au, Ag, CoO, MoS_2 etc.) can be added to accelerate the surface reaction rate; nanostructure morphologies with more exposed surfaces (e.g., nanosheets, nanoplatelets) and facets can be synthesized to increase the surface area and density of reaction sites; novel heterojunctions can be formed to enhance the charge separation.

3. Expanding the scope of organic transformations and develop new key chemical reactions. Several organic transformations have been reported to date, such as benzyl alcohol oxidation and C−H, C−O, and C−N bond activations. Unlike H_2 generation and CO_2 reduction, MHPs offer an impressive activity on organic transformations (TON over 52 000 for α-alkylation of aldehydes on $CsPbBr_3$,[65] 32 900 μmol/g/h of acetophenone generation rate on $Cs_3Bi_2Br_9$-based photocatalyst[78]). However, the reported organic transformations with MHP photocatalysts are narrow, in comparison to known heterogeneous and homogeneous photocatalytic organic synthesis by other semiconductor photocatalysts[115] or molecule photoredox catalysts.[116,117] Expanding the photoredox reaction scope of MHPs by combining them with other molecule catalysts, such as Ir, Ru, and Ni complexes, can be promising for the high value-added organic synthesis. Further, aiming for high specificity and stereoselectivity is a promising direction for MHP-based photoredox catalysis.

4. Enhancing the redox ability of MHP-based photocatalysis. The relatively narrow bandgaps of MHPs will inevitably bring about weak redox abilities and, specifically related to the VB edge, poor oxidation abilities. Some oxidation reactions, like water oxidation (1.23 eV vs RHE for H_2O/O_2) or volatile organic compound mineralization (1.67 eV vs RHE for $OH^-/^\bullet OH$), will challenge the oxidation ability of the small bandgap MHP. By combination with other semiconductors with a more positive VB to build heterostructure (generating a Z-scheme), an alternate pathway to achieve broad light absorption and strong redox ability is possible. Alternatively, by developing the MHP-based PEC reaction system (via encapsulating the perovskite layer in a solar cell architecture), the applied voltage can enhance the redox ability of the MHP to achieve a broad reaction scope.

The general performance and stability of MHP-based photocatalysts are currently far from optimal, limiting their ability to address society's energy and environmental concerns effectively. The current state of the art demonstrates that this emerging technology does hold promise, driven by similar motives of other popular MHP-based optoelectronic applications: easy, low-cost materials processing coupled with interesting photophysical properties. The field of MHP-based photocatalysis is still in a relatively early stage of discovery, and this Review is intended to serve as a general guiding tool toward finding optimal photocatalytic performance and stability.

AUTHOR INFORMATION

Corresponding Authors

Maarten B. J. Roeffaers − *cMACS, Department of Microbial and Molecular Systems, KU Leuven, 3001 Leuven, Belgium;* Email: maarten.roeffaers@kuleuven.be
Julian A. Steele − *cMACS, Department of Microbial and Molecular Systems, KU Leuven, 3001 Leuven, Belgium;* orcid.org/0000-0001-7982-4413; Email: julian.steele@kuleuven.be

Authors

Haowei Huang − *cMACS, Department of Microbial and Molecular Systems, KU Leuven, 3001 Leuven, Belgium*
Bapi Pradhan − *Department of Chemistry, KU Leuven, 3001 Heverlee, Belgium;* orcid.org/0000-0002-6202-7343
Johan Hofkens − *Department of Chemistry, KU Leuven, 3001 Heverlee, Belgium;* orcid.org/0000-0002-9101-0567

Complete contact information is available at:
https://pubs.acs.org/10.1021/acsenergylett.0c00058

Notes

The authors declare no competing financial interest.

Biographies

Haowei Huang received his masters degrees from Fuzhou University (China) and University of York (U.K.). At the end of 2016, he joined the group of Prof. Roeffaers (KU Leuven, Belgium) as a Ph.D. student (Marie Curie ESR) with financial support from Marie Sklodowska-Curie innovation program where he is mainly working on perovskites photocatalysis.

Bapi Pradhan received his M.Sc. in chemistry from Indian Institute of Technology, Bombay, and Ph.D. degree from Indian Association for the Cultivation of Science. Currently, he is working as a postdoc at KU

Leuven in the group of Prof. Hofkens on the optoelectronic applications of metal halide perovskites.

Johan Hofkens graduated from the Laboratory of Photochemistry and Spectroscopy, KU Leuven (Belgium), in 1993 studying TICT-states in organic molecules by time-resolved fluorescence measurements. After a postdoctoral stay (1994−1995) with Prof. Masuhara at Osaka University (Japan) on the development of optical trapping and with the late Prof. Barbara at University of Minneapolis (United States) on single-molecule spectroscopy, he returned to the KU Leuven were he started the single-molecule group, focusing on the development of optical microscopy tools to study challenging topics at the boundary of chemistry, biology, and physics.

Maarten B. J. Roeffaers graduated from the Centre for Surface Chemistry and Catalysis, KU Leuven (Belgium), in 2008 studying zeolite catalysis with fluorescence microscopy. After a postdoctoral stay (2009−2010) with Prof. Xie at Harvard University (United States) on the development and use of coherent Raman microscopy, he returned to the KU Leuven. In 2010, he started his own research group (www.roeffaers-lab.org) focusing on the development of optical microscopy tools to study heterogeneous catalysis and optically active materials such as Ag-zeolites and metal-halide perovskites.

Julian A. Steele received his Ph.D. in solid-state physics from The Institute for Superconducting and Electronic Materials, University of Wollongong, in 2016 and then joined the group of Prof. Roeffaers (KU Leuven) as a postdoctoral researcher with financial support from the Belgium government (FWO), where his work focuses on nanoscale optical materials.

■ ACKNOWLEDGMENTS

The authors acknowledge financial support from the Research Foundation - Flanders (FWO) through a postdoctoral fellowship to J.A.S. (FWO Grant No. 12Y7218N) and research projects to J.H. and M.B.J.R (FWO Grant Nos. G098319N and ZW15_09-GOH6316), the European Union (Horizon 2020) Marie Sklodowska-Curie innovation program (Grant No. 722591 and a Ph.D. fellowship to H.H.), the KU Leuven Research Fund (C14/15/053 and C14/19/079), and the Flemish government through long term structural funding Methusalem (CASAS2, Meth/15/04).

■ REFERENCES

(1) Kim, D.; Sakimoto, K. K.; Hong, D.; Yang, P. Artificial Photosynthesis for Sustainable Fuel and Chemical Production. *Angew. Chem., Int. Ed.* **2015**, *54*, 3259−3266.

(2) Kamat, P. V. Meeting the Clean Energy Demand: Nanostructure Architectures for Solar Energy Conversion. *J. Phys. Chem. C* **2007**, *111*, 2834−2860.

(3) Fujishima, A.; Honda, K. Electrochemical Photolysis of Water at a Semiconductor Electrode. *Nature* **1972**, *238*, 37−38.

(4) Hisatomi, T.; Kubota, J.; Domen, K. Understanding TiO_2 Photocatalysis: Mechanisms and Materials. *Chem. Soc. Rev.* **2014**, *43*, 7520−7535.

(5) Zhou, H.; Qu, Y.; Zeid, T.; Duan, X. Towards highly efficient photocatalysts using semiconductor nanoarchitectures. *Energy Environ. Sci.* **2012**, *5*, 6732−6743.

(6) Ge, M.; Li, Q.; Cao, C.; Huang, J.; Li, S.; Zhang, S.; Chen, Z.; Zhang, K.; Al-Deyab, S. S.; Lai, Y. Lai, One-dimensional TiO_2 Nanotube Photocatalysts for Solar Water Splitting. *Adv. Sci.* **2017**, *4*, 1600152.

(7) Wen, J.; Xie, J.; Chen, X.; Li, X. A review on g-C_3N_4-based photocatalysts. *Appl. Surf. Sci.* **2017**, *391*, 72−123.

(8) He, R. a.; Cao, S.; Zhou, P.; Yu, J. Recent advances in visible light Bi-based photocatalysts. *Chin. J. Catal.* **2014**, *35*, 989−1007.

(9) Elumalai, N. K.; Mahmud, M. A.; Wang, D.; Uddin, A. Perovskite Solar Cells: Progress and Advancements. *Energies* **2016**, *9*, 861.

(10) Wu, Y.; Chen, W.; Chen, G.; Liu, L.; He, Z.; Liu, R. The Impact of Hybrid Compositional Film/Structure on Organic−Inorganic Perovskite Solar Cells. *Nanomaterials* **2018**, *8*, 356.

(11) Tamirat, A. G.; Rick, J.; Dubale, A. A.; Su, W.-N.; Hwang, B.-J. Using hematite for photoelectrochemical water splitting: a review of current progress and challenges. *Nanoscale Horiz.* **2016**, *1*, 243−267.

(12) Hendon, C. H.; Tiana, D.; Fontecave, M.; Sanchez, C.; D'arras, L.; Sassoye, C.; Rozes, L.; Mellot-Draznieks, C.; Walsh, A. Engineering the Optical Response of the Titanium-MIL-125 Metal−Organic Framework through Ligand Functionalization. *J. Am. Chem. Soc.* **2013**, *135*, 10942−10945.

(13) Jiang, Y.; Cho, S.-Y.; Shim, M. Light-emitting diodes of colloidal quantum dots and nanorod heterostructures for future emissive displays. *J. Mater. Chem. C* **2018**, *6*, 2618−2634.

(14) Kibria, M. G.; Mi, Z. Artificial photosynthesis using metal/nonmetal-nitride semiconductors: current status, prospects, and challenges. *J. Mater. Chem. A* **2016**, *4*, 2801−2820.

(15) Wang, Y.; Zhang, Z.; Zhang, L.; Luo, Z.; Shen, J.; Lin, H.; Long, J.; Wu, J. C. S.; Fu, X.; Wang, X.; Li, C. Visible-Light Driven Overall Conversion of CO_2 and H_2O to CH_4 and O_2 on 3D-SiC@2D-MoS_2 Heterostructure. *J. Am. Chem. Soc.* **2018**, *140*, 14595−14598.

(16) Xie, S.; Zhang, Q.; Liu, G.; Wang, Y. Photocatalytic and photoelectrocatalytic reduction of CO_2 using heterogeneous catalysts with controlled nanostructures. *Chem. Commun.* **2016**, *52*, 35−39.

(17) Wu, J.; Huang, Y.; Ye, W.; Li, Y. CO_2 Reduction: From the Electrochemical to Photochemical Approach. *Adv. Sci.* **2017**, *4*, 1700194.

(18) Xiao, X.; Jiang, J.; Zhang, L. Selective oxidation of benzyl alcohol into benzaldehyde over semiconductors under visible light: The case of $Bi_{12}O_{17}Cl_2$ nanobelts. *Appl. Catal., B* **2013**, *142−143*, 487.

(19) Kong, D.; Zheng, Y.; Kobielusz, M.; Wang, Y.; Bai, Z.; Macyk, W.; Wang, X.; Tang, J. Recent advances in visible light-driven water oxidation and reduction in suspension systems. *Mater. Today* **2018**, *21*, 897−924.

(20) Li, X.; Yu, J.; Jaroniec, M. Hierarchical photocatalysts. *Chem. Soc. Rev.* **2016**, *45*, 2603−2636.

(21) Stranks, S. D.; Snaith, H. J. Metal-halide perovskites for photovoltaic and light-emitting devices. *Nat. Nanotechnol.* **2015**, *10*, 391−402.

(22) Ha, S.-T.; Su, R.; Xing, J.; Zhang, Q.; Xiong, Q. Metal halide perovskite nanomaterials: synthesis and applications. *Chem. Sci.* **2017**, *8*, 2522−2536.

(23) Brenner, T. M.; Egger, D. A.; Kronik, L.; Hodes, G.; Cahen, D. Hybrid organic-inorganic perovskites: low-cost semiconductors with intriguing charge-transport properties. *Nat. Rev. Mater.* **2016**, *1*, 15007.

(24) Mosconi, E.; Amat, A.; Nazeeruddin, M. K.; Grätzel, M.; De Angelis, F. First-Principles Modeling of Mixed Halide Organometal Perovskites for Photovoltaic Applications. *J. Phys. Chem. C* **2013**, *117*, 13902−13913.

(25) Herz, L. M. Charge-Carrier Dynamics in Organic-Inorganic Metal Halide Perovskites. *Annu. Rev. Phys. Chem.* **2016**, *67*, 65−89.

(26) Wehrenfennig, C.; Eperon, G. E.; Johnston, M. B.; Snaith, H. J.; Herz, L. M. High Charge Carrier Mobilities and Lifetimes in Organolead Trihalide Perovskites. *Adv. Mater.* **2014**, *26*, 1584−1589.

(27) Jin, H.; Debroye, E.; Keshavarz, M.; Scheblykin, I. G.; Roeffaers, M. B. J.; Hofkens, J.; Steele, J. A. It's a trap! On the nature of localised states and charge trapping in lead halide perovskites. *Mater. Horiz.* **2020**, *7*, 397−410.

(28) Park, S.; Chang, W. J.; Lee, C. W.; Park, S.; Ahn, H. Y.; Nam, K. T. Photocatalytic hydrogen generation from hydriodic acid using methylammonium lead iodide in dynamic equilibrium with aqueous solution. *Nat. Energy* **2017**, *2*, 16185.

(29) Quan, L. N.; García de Arquer, F. P.; Sabatini, R. P.; Sargent, E. H. Metal-halide perovskites for photovoltaic and light-emitting devices. *Adv. Mater.* **2018**, *30*, 1801996.

(30) Wang, R.; Mujahid, M.; Duan, Y.; Wang, Z.-K.; Xue, J.; Yang, Y. A Review of Perovskites Solar Cell Stability. *Adv. Funct. Mater.* **2019**, *29*, 1808843.

(31) Yang, W. S.; Noh, J. H.; Jeon, N. J.; Kim, Y. C.; Ryu, S.; Seo, J.; Seok, S. I. High-performance photovoltaic perovskite layers fabricated through intramolecular exchange. *Science* **2015**, *348*, 1234−1237.

(32) Zhu, Z.; Hadjiev, V. G.; Rong, Y.; Guo, R.; Cao, B.; Tang, Z.; Qin, F.; Li, Y.; Wang, Y.; Hao, F.; Venkatesan, S.; Li, W.; Baldelli, S.; Guloy, A. M.; Fang, H.; Hu, Y.; Yao, Y.; Wang, Z.; Bao, J. Interaction of Organic Cation with Water Molecule in Perovskite $MAPbI_3$: From Dynamic Orientational Disorder to Hydrogen Bonding. *Chem. Mater.* **2016**, *28*, 7385−7393.

(33) Murali, B.; Dey, S.; Abdelhady, A. L.; Peng, W.; Alarousu, E.; Kirmani, A. R.; Cho, N.; Sarmah, S. P.; Parida, M. R.; Saidaminov, M. I.; Zhumekenov, A. A.; Sun, J.; Alias, M. S.; Yengel, E.; Ooi, B. S.; Amassian, A.; Bakr, O. M.; Mohammed, O. F. Surface Restructuring of Hybrid Perovskite Crystals. *ACS Energy Lett.* **2016**, *1*, 1119−1126.

(34) Kwon, Y. S.; Lim, J.; Yun, H.-J.; Kim, Y.-H.; Park, T. A diketopyrrolopyrrole-containing hole transporting conjugated polymer for use in efficient stable organic-inorganic hybrid solar cells based on a perovskite. *Energy Environ. Sci.* **2014**, *7*, 1454−1460.

(35) Christians, J. A.; Miranda Herrera, P. A.; Kamat, P. V. Transformation of the Excited State and Photovoltaic Efficiency of $CH_3NH_3PbI_3$ Perovskite upon Controlled Exposure to Humidified Air. *J. Am. Chem. Soc.* **2015**, *137*, 1530−1538.

(36) Yang, J.; Siempelkamp, B. D.; Liu, D.; Kelly, T. L. Investigation of $CH_3NH_3PbI_3$ Degradation Rates and Mechanisms in Controlled Humidity Environments Using *in Situ* Techniques. *ACS Nano* **2015**, *9*, 1955−1963.

(37) Mosconi, E.; Azpiroz, J. M.; De Angelis, F. Ab Initio Molecular Dynamics Simulations of Methylammonium Lead Iodide Perovskite Degradation by Water. *Chem. Mater.* **2015**, *27*, 4885−4892.

(38) Niu, G.; Guo, X.; Wang, L. Review of recent progress in chemical stability of perovskite solar cells. *J. Mater. Chem. A* **2015**, *3*, 8970−8980.

(39) Huang, J. B.; Tan, S. Q.; Lund, P. D.; Zhou, H. P. Impact of H_2O on organic-inorganic hybrid perovskite solar cells. *Energy Environ. Sci.* **2017**, *10*, 2284−2311.

(40) Boyd, C. C.; Cheacharoen, R.; Leijtens, T.; McGehee, M. D. Understanding Degradation Mechanisms and Improving Stability of Perovskite Photovoltaics. *Chem. Rev.* **2019**, *119*, 3418−3451.

(41) El-Mellouhi, F.; Marzouk, A.; Bentria, E. T.; Rashkeev, S. N.; Kais, S.; Alharbi, F. H. Hydrogen Bonding and Stability of Hybrid Organic-Inorganic Perovskites. *ChemSusChem* **2016**, *9*, 2648−2655.

(42) Manser, J. S.; Saidaminov, M. I.; Christians, J. A.; Bakr, O. M.; Kamat, P. V. Making and Breaking of Lead Halide Perovskites. *Acc. Chem. Res.* **2016**, *49*, 330−338.

(43) Jeon, N. J.; Noh, J. H.; Kim, Y. C.; Yang, W. S.; Ryu, S.; Seok, S. I. Solvent engineering for high-performance inorganic−organic hybrid perovskite solar cells. *Nat. Mater.* **2014**, *13*, 897.

(44) Jung, M.; Ji, S.-G.; Kim, G.; Seok, S. I. Perovskite precursor solution chemistry: from fundamentals to photovoltaic applications. *Chem. Soc. Rev.* **2019**, *48*, 2011−2038.

(45) Noel, N. K.; Habisreutinger, S. N.; Wenger, B.; Klug, M. T.; Hörantner, M. T.; Johnston, M. B.; Nicholas, R. J.; Moore, D. T.; Snaith, H. J. A low viscosity, low boiling point, clean solvent system for the rapid crystallisation of highly specular perovskite films. *Energy Environ. Sci.* **2017**, *10*, 145−152.

(46) Pearson, A. J.; Eperon, G. E.; Hopkinson, P. E.; Habisreutinger, S. N.; Wang, J. T. W.; Snaith, H. J.; Greenham, N. C. Oxygen Degradation in Mesoporous $Al_2O_3/CH_3NH_3PbI_{3-x}Cl_x$ Perovskite Solar Cells: Kinetics and Mechanisms. *Adv. Energy Mater.* **2016**, *6*, 1600014.

(47) Abdelmageed, G.; Jewell, L.; Hellier, K.; Seymour, L.; Luo, B.; Bridges, F.; Zhang, J. Z.; Carter, S. Mechanisms for light induced degradation in MAPbI3 perovskite thin films and solar cells. *Appl. Phys. Lett.* **2016**, *109*, 233905.

(48) Aristidou, N.; Eames, C.; Sanchez-Molina, I.; Bu, X. N.; Kosco, J.; Islam, M. S.; Haque, S. A. Fast oxygen diffusion and iodide defects mediate oxygen-induced degradation of perovskite solar cells. *Nat. Commun.* **2017**, *8*, 15218.

(49) Kulbak, M.; Gupta, S.; Kedem, N.; Levine, I.; Bendikov, T.; Hodes, G.; Cahen, D. Cesium enhances long-term stability of lead bromide perovskite-based solar cells. *J. Phys. Chem. Lett.* **2016**, *7*, 167−172.

(50) Lee, J. W.; Kim, D. H.; Kim, H. S.; Seo, S. W.; Cho, S. M.; Park, N. G. Formamidinium and cesium hybridization for photo-and moisture-stable perovskite solar cell. *Adv. Energy Mater.* **2015**, *5*, 1501310.

(51) Zheng, C.; Rubel, O. Ionization Energy as a Stability Criterion for Halide Perovskites. *J. Phys. Chem. C* **2017**, *121* (22), 11977−11984.

(52) Kim, Y.; Yassitepe, E.; Voznyy, O.; Comin, R.; Walters, G.; Gong, X.; Kanjanaboos, P.; Nogueira, A. F.; Sargent, E. H. Efficient Luminescence from Perovskite Quantum Dot Solids. *ACS Appl. Mater. Interfaces* **2015**, *7*, 25007−25013.

(53) Wu, Y.; Wang, P.; Zhu, X.; Zhang, Q.; Wang, Z.; Liu, Y.; Zou, G.; Dai, Y.; Whangbo, M.-H.; Huang, B. Composite of $CH_3NH_3PbI_3$ with Reduced Graphene Oxide as a Highly Efficient and Stable Visible-Light Photocatalyst for Hydrogen Evolution in Aqueous HI Solution. *Adv. Mater.* **2018**, *30*, 1704342.

(54) Wu, Y.; Wang, P.; Guan, Z.; Liu, J.; Wang, Z.; Zheng, Z.; Jin, S.; Dai, Y.; Whangbo, M.-H.; Huang, B. Enhancing the Photocatalytic Hydrogen Evolution Activity of Mixed-Halide Perovskite $CH_3NH_3PbBr_{3-x}I_x$ Achieved by Bandgap Funneling of Charge Carriers. *ACS Catal.* **2018**, *8*, 10349−10357.

(55) Guan, Z.; Wu, Y.; Wang, P.; Zhang, Q.; Wang, Z.; Zheng, Z.; Liu, Y.; Dai, Y.; Whangbo, M.-H.; Huang, B. Perovskite photocatalyst $CsPbBr_{3-x}I_x$ with a bandgap funnel structure for H_2 evolution under visible light. *Appl. Catal., B* **2019**, *245*, 522−527.

(56) Wang, H.; Wang, X.; Chen, R.; Zhang, H.; Wang, X.; Wang, J.; Zhang, J.; Mu, L.; Wu, K.; Fan, F.; Zong, X.; Li, C. Promoting Photocatalytic H_2 Evolution on Organic−Inorganic Hybrid Perovskite Nanocrystals by Simultaneous Dual-Charge Transportation Modulation. *ACS Energy Lett.* **2019**, *4*, 40−47.

(57) Wang, X.; Wang, H.; Zhang, H.; Yu, W.; Wang, X.; Zhao, Y.; Zong, X.; Li, C. Dynamic Interaction between Methylammonium Lead Iodide and TiO_2 Nanocrystals Leads to Enhanced Photocatalytic H_2 Evolution from HI Splitting. *ACS Energy Lett.* **2018**, *3*, 1159−1164.

(58) Luo, J.; Yang, H.; Liu, Z.; Li, F.; Liu, S.; Ma, J.; Liu, B. Organic-inorganic hybrid perovskite - TiO_2 nanorod arrays for efficient and stable photoelectrochemical hydrogen evolution from HI splitting. *Mater. Today Chem.* **2019**, *12*, 1−6.

(59) Li, R.; Li, X.; Wu, J.; Lv, X.; Zheng, Y.-Z.; Zhao, Z.; Ding, X.; Tao, X.; Chen, J.-F. Few-layer black phosphorus-on-$MAPbI_3$ for superb visible-light photocatalytic hydrogen evolution from HI splitting. *Appl. Catal., B* **2019**, *259*, 118075.

(60) Guo, Y.; Liu, G.; Li, Z.; Lou, Y.; Chen, J.; Zhao, Y. Stable Lead-Free $(CH_3NH_3)_3Bi_2I_9$ Perovskite for Photocatalytic Hydrogen Generation. *ACS Sustainable Chem. Eng.* **2019**, *7*, 15080−15085.

(61) Wang, T.; Yue, D.; Li, X.; Zhao, Y. Lead-free double perovskite $Cs_2AgBiBr_6$/RGO composite for efficient visible light photocatalytic H_2 evolution. *Appl. Catal., B* **2020**, *268*, 118399.

(62) Xu, Y. F.; Yang, M. Z.; Chen, B. X.; Wang, X. D.; Chen, H. Y.; Kuang, D. B.; Su, C. Y. A $CsPbBr_3$ Perovskite Quantum Dot/Graphene Oxide Composite for Photocatalytic CO_2 Reduction. *J. Am. Chem. Soc.* **2017**, *139*, 5660−5663.

(63) Huang, H.; Yuan, H.; Janssen, K. P. F.; Solís-Fernández, G.; Wang, Y.; Tan, C. Y. X.; Jonckheere, D.; Debroye, E.; Long, J.; Hendrix, J.; Hofkens, J.; Steele, J. A.; Roeffaers, M. B. J. Efficient and Selective Photocatalytic Oxidation of Benzylic Alcohols with Hybrid Organic−Inorganic Perovskite Materials. *ACS Energy Lett.* **2018**, *3*, 755−759.

(64) Huang, H.; Yuan, H.; Zhao, J.; Solís-Fernández, G.; Zhou, C.; Seo, J. W.; Hendrix, J.; Debroye, E.; Steele, J. A.; Hofkens, J.; Long, J.; Roeffaers, M. B. J $C(sp^3)$-H Bond Activation by Perovskite Solar Photocatalyst Cell. *ACS Energy Lett.* **2019**, *4*, 203−208.

(65) Zhu, X.; Lin, Y.; San Martin, J.; Sun, Y.; Zhu, D.; Yan, Y. Lead halide perovskites for photocatalytic organic synthesis. *Nat. Commun.* **2019**, *10*, 2843.

(66) Zhu, X.; Lin, Y.; Sun, Y.; Beard, M. C.; Yan, Y. Lead-Halide Perovskites for Photocatalytic α-Alkylation of Aldehydes. *J. Am. Chem. Soc.* **2019**, *141*, 733−738.

(67) Chen, K.; Deng, X. H.; Dodekatos, G.; Tüysüz, H. Photocatalytic Polymerization of 3,4-Ethylenedioxythiophene over Cesium Lead Iodide Perovskite Quantum Dots. *J. Am. Chem. Soc.* **2017**, *139*, 12267−12273.

(68) Wu, W. B.; Wong, Y. C.; Tan, Z. K.; Wu, J. Photo-induced thiol coupling and C-H activation using nanocrystalline lead-halide perovskite catalysts. *Catal. Sci. Technol.* **2018**, *8*, 4257−4263.

(69) Ou, M.; Tu, W.; Yin, S.; Xing, W.; Wu, S.; Wang, H.; Wan, S.; Zhong, Q.; Xu, R. Amino-Assisted Anchoring of $CsPbBr_3$ Perovskite Quantum Dots on Porous g-C_3N_4 for Enhanced Photocatalytic CO_2 Reduction. *Angew. Chem.* **2018**, *130*, 13758−13762.

(70) Guo, S.-H.; Zhou, J.; Zhao, X.; Sun, C.-Y.; You, S.-Q.; Wang, X.-L.; Su, Z.-M. Enhanced CO_2 photoreduction via tuning halides in perovskites. *J. Catal.* **2019**, *369*, 201−208.

(71) Hou, J.; Cao, S.; Wu, Y.; Gao, Z.; Liang, F.; Sun, Y.; Lin, Z.; Sun, L. Inorganic Colloidal Perovskite Quantum Dots for Robust Solar CO_2 Reduction. *Chem. - Eur. J.* **2017**, *23*, 9481−9485.

(72) Zhou, L.; Xu, Y.-F.; Chen, B.-X.; Kuang, D.-B.; Su, C.-Y. Synthesis and Photocatalytic Application of Stable Lead-Free $Cs_2AgBiBr_6$ Perovskite Nanocrystals. *Small* **2018**, *14*, 1703762.

(73) Pan, A.; Ma, X.; Huang, S.; Wu, Y.; Jia, M.; Shi, Y.; Liu, Y.; Wangyang, P.; He, L.; Liu, Y. $CsPbBr_3$ Perovskite Nanocrystal Grown on MXene Nanosheets for Enhanced Photoelectric Detection and Photocatalytic CO_2 Reduction. *J. Phys. Chem. Lett.* **2019**, *10*, 6590−6597.

(74) Cardenas-Morcoso, D.; Gualdrón-Reyes, A. F.; Ferreira Vitoreti, A. B.; García-Tecedor, M.; Yoon, S. J.; Solis de la Fuente, M.; Mora-Seró, I.; Gimenez, S. Photocatalytic and Photoelectrochemical Degradation of Organic Compounds with All-Inorganic Metal Halide Perovskite Quantum Dots. *J. Phys. Chem. Lett.* **2019**, *10*, 630−636.

(75) Guo, X.-X.; Tang, S.-F.; Mu, Y.-F.; Wu, L.-Y.; Dong, G.-X.; Zhang, M. Engineering a $CsPbBr_3$-based nanocomposite for efficient photocatalytic CO_2 reduction: improved charge separation concomitant with increased activity sites. *RSC Adv.* **2019**, *9*, 34342−34348.

(76) Feng, X.; Ju, H.; Song, T.; Fang, T.; Liu, W.; Huang, W. Highly Efficient Photocatalytic Degradation Performance of $CsPb(Br_{1-x}Cl_x)_3$-Au Nanoheterostructures. *ACS Sustainable Chem. Eng.* **2019**, *7*, 5152−5156.

(77) Gualdrón Reyes, A. F.; Rodriguez-Pereira, J.; Amado - Gonzalez, E.; Rueda-P, J.; Ospina, R.; Masi, S.; Yoon, S. J.; Tirado, J.; Jaramillo, F.; Agouram, S.; Munoz-Sanjose, V.; Gimenez, S.; Mora-Seró, I. Unravelling the Photocatalytic Behavior of All-Inorganic Mixed Halide Perovskites: The Role of Surface Chemical States. *ACS Appl. Mater. Interfaces* **2020**, *12*, 914−924.

(78) Dai, Y.; Poidevin, C.; Ochoa-Hernández, C.; Auer, A.; Tüysüz, H. Supported bismuth halide perovskite photocatalyst for selective aliphatic and aromatic C-H bond activation. *Angew. Chem., Int. Ed.* **2020**, *59*, 2−11.

(79) Schünemann, S.; van Gastel, M.; Tüysüz, H. A $CsPbBr_3$ /TiO_2 Composite for Visible-Light-Driven Photocatalytic Benzyl Alcohol Oxidation. *ChemSusChem* **2018**, *11*, 2057−2061.

(80) Hong, Z.; Chong, W. K.; Ng, A. Y. R.; Li, M.; Ganguly, R.; Sum, T. C.; Soo, H. S. Hydrophobic Metal Halide Perovskites for Visible-Light Photoredox C-C Bond Cleavage and Dehydrogenation Catalysis. *Angew. Chem., Int. Ed.* **2019**, *58*, 3456−3460.

(81) Xu, Y.-F.; Wang, X.-D.; Liao, J.-F.; Chen, B.-X.; Chen, H.-Y.; Kuang, D.-B. Amorphous-TiO_2-Encapsulated $CsPbBr_3$ Nanocrystal Composite Photocatalyst with Enhanced Charge Separation and CO_2 Fixation. *Adv. Mater. Interfaces* **2018**, *5*, 1801015.

(82) Li, Z.-J.; Hofman, E.; Li, J.; Davis, A. H.; Tung, C.-H.; Wu, L.-Z.; Zheng, W. Photoelectrochemically Active and Environmentally Stable $CsPbBr_3$/TiO_2 Core/Shell Nanocrystals. *Adv. Funct. Mater.* **2018**, *28*, 1704288.

(83) Wu, L.-Y.; Mu, Y.-F.; Guo, X.-X.; Zhang, W.; Zhang, Z.-M.; Zhang, M.; Lu, T.-B. Encapsulating Perovskite Quantum Dots in Iron-Based Metal-Organic Frameworks (MOFs) for Efficient Photocatalytic CO_2 Reduction. *Angew. Chem., Int. Ed.* **2019**, *58*, 9491−9495.

(84) Kong, Z.-C.; Liao, J.-F.; Dong, Y.-J.; Xu, Y.-F.; Chen, H.-Y.; Kuang, D.-B.; Su, C.-Y. Core@Shell $CsPbBr_3$@Zeolitic Imidazolate Framework Nanocomposite for Efficient Photocatalytic CO_2 Reduction. *ACS Energy Lett.* **2018**, *3*, 2656−2662.

(85) Nam, S.; Mai, C. T. K.; Oh, I. Ultrastable Photoelectrodes for Solar Water Splitting Based on Organic Metal Halide Perovskite Fabricated by Lift-Off Process. *ACS Appl. Mater. Interfaces* **2018**, *10*, 14659−14664.

(86) Mollick, S.; Mandal, T. N.; Jana, A.; Fajal, S.; Desai, A. V.; Ghosh, S. K. Ultrastable Luminescent Hybrid Bromide Perovskite@MOF Nanocomposites for the Degradation of Organic Pollutants in Water. *ACS Appl. Nano Mater.* **2019**, *2*, 1333−1340.

(87) Chen, Y. S.; Manser, J. S.; Kamat, P. V. All Solution-Processed Lead Halide Perovskite-BiVO4 Tandem Assembly for Photolytic Solar Fuels Production. *J. Am. Chem. Soc.* **2015**, *137*, 974−981.

(88) Da, P. M.; Cha, M. Y.; Sun, L.; Wu, Y. Z.; Wang, Z. S.; Zheng, G. F. High-Performance Perovskite Photoanode Enabled by Ni Passivation and Catalysis. *Nano Lett.* **2015**, *15*, 3452−3457.

(89) Gurudayal; Sabba, D.; Kumar, M. H.; Wong, L. H.; Barber, J.; Gratzel, M.; Mathews, N. Perovskite-Hematite Tandem Cells for Efficient Overall Solar Driven Water Splitting. *Nano Lett.* **2015**, *15*, 3833−3839.

(90) Luo, J. S.; Im, J. H.; Mayer, M. T.; Schreier, M.; Nazeeruddin, M. K.; Park, N. G.; Tilley, S. D.; Fan, H. J.; Gratzel, M. Water photolysis at 12.3% efficiency via perovskite photovoltaics and Earth-abundant catalysts. *Science* **2014**, *345*, 1593−1596.

(91) Crespo-Quesada, M.; Pazos-Outon, L. M.; Warnan, J.; Kuehnel, M. F.; Friend, R. H.; Reisner, E. Metal-encapsulated organolead halide perovskite photocathode for solar-driven hydrogen evolution in water. *Nat. Commun.* **2016**, *7*, 12555.

(92) Mu, Y.-F.; Zhang, W.; Guo, X.-X.; Dong, G.-X.; Zhang, M.; Lu, T.-B. Water-Tolerant Lead Halide Perovskite Nanocrystals as Efficient Photocatalysts for Visible-Light-Driven CO_2 Reduction in Pure Water. *ChemSusChem* **2019**, *12*, 4769−4774.

(93) Andrei, V.; Reuillard, B.; Reisner, E. Bias-free solar syngas production by integrating a molecular cobalt catalyst with perovskite−$BiVO_4$ tandems. *Nat. Mater.* **2020**, *19*, 189−194.

(94) Poli, I.; Hintermair, U.; Regue, M.; Kumar, S.; Sackville, E. V.; Baker, J.; Watson, T. M.; Eslava, S.; Cameron, P. J. Graphite-protected $CsPbBr_3$ perovskite photoanodes functionalised with water oxidation catalyst for oxygen evolution in water. *Nat. Commun.* **2019**, *10*, 2097.

(95) Wang, Q.; Qin, W.; Wu, X.; Yu, S. Isopropanol-assisted synthesis of highly stable $MAPbBr_3$/p-g-C_3N_4 intergrowth composite photocatalysts and their interfacial charge carrier dynamics. *Nanoscale Adv.* **2020**, *2*, 274−285.

(96) Jiang, Y.; Liao, J.-F.; Xu, Y.-F.; Chen, H.-Y.; Wang, X.-D.; Kuang, D.-B. Hierarchical $CsPbBr_3$ nanocrystal-decorated ZnO nanowire/macroporous graphene hybrids for enhancing charge separation and photocatalytic CO_2 reduction. *J. Mater. Chem. A* **2019**, *7*, 13762−13769.

(97) Wang, X.-D.; Huang, Y.-H.; Liao, J.-F.; Jiang, Y.; Zhou, L.; Zhang, X.-Y.; Chen, H.-Y.; Kuang, D.-B. In Situ Construction of a Cs_2SnI_6 Perovskite Nanocrystal/SnS_2 Nanosheet Heterojunction with Boosted Interfacial Charge Transfer. *J. Am. Chem. Soc.* **2019**, *141*, 13434−13441.

(98) Bhosale, S. S.; Kharade, A. K.; Jokar, E.; Fathi, A.; Chang, S.-m.; Diau, E. W. -G. Mechanism of Photocatalytic CO_2 Reduction by Bismuth-Based Perovskite Nanocrystals at the Gas−Solid Interface. *J. Am. Chem. Soc.* **2019**, *141* (51), 20434−20442.

(99) Reyes-Pérez, F.; Gallardo, J. J.; Aguilar, T.; Alcántara, R.; Fernández-Lorenzo, C.; Navas, J. Visible-Light-Enhanced Photocatalytic Activity of Totally Inorganic Halide-Based Perovskite. *Chemistry Select* **2018**, *3*, 10226−10235.

(100) Zhang, Z.; Liang, Y.; Huang, H.; Liu, X.; Li, Q.; Chen, L.; Xu, D. Stable and Highly Efficient Photocatalysis with Lead-Free Double-Perovskite of $Cs_2AgBiBr_6$. *Angew. Chem., Int. Ed.* **2019**, *58*, 7263−7267.

(101) Dai, Y.; Tüysüz, H. Lead-Free $Cs_3Bi_2Br_9$ Perovskiteas Photocatalyst for Ring-Opening Reactions of Epoxides. *ChemSusChem* **2019**, *12*, 2587−2592.

(102) Qian, X.; Chen, Z.; Yang, X.; Zhao, W.; Liu, C.; Sun, T.; Zhou, D.; Yang, Q.; Wei, G.; Fan, M. Perovskite cesium lead bromide

quantum dots: A new efficient photocatalyst for degrading antibiotic residues in organic system. *J. Cleaner Prod.* **2020**, *249*, 119335.

(103) Schneider, J.; Bahnemann, D. W. Undesired Role of Sacrificial Reagents in Photocatalysis. *J. Phys. Chem. Lett.* **2013**, *4*, 3479−3483.

(104) Yang, J.; Wang, D.; Han, H.; Li, C. Roles of Cocatalysts in Photocatalysis and Photoelectrocatalysis. *Acc. Chem. Res.* **2013**, *46*, 1900−1909.

(105) Panayotov, D. A.; Frenkel, A. I.; Morris, J. R. Catalysis and Photocatalysis by Nanoscale Au/TiO_2: Perspectives for Renewable Energy. *ACS Energy Lett.* **2017**, *2*, 1223−1231.

(106) Yan, J.; Qiu, W.; Wu, G.; Heremans, P.; Chen, H. Recent progress in 2D/quasi-2D layered metal halide perovskites for solar cells. *J. Mater. Chem. A* **2018**, *6*, 11063−11077.

(107) Andrei, V.; Hoye, R. L. Z.; Crespo-Quesada, M.; Bajada, M.; Ahmad, S.; De Volder, M.; Friend, R.; Reisner, E. Scalable Triple Cation Mixed Halide Perovskite-$BiVO_4$ Tandems for Bias-Free Water Splitting. *Adv. Energy Mater.* **2018**, *8*, 1801403.

(108) Gupta, S.; Bendikov, T.; Hodes, G.; Cahen, D. $CsSnBr_3$, A Lead-Free Halide Perovskite for Long-Term Solar Cell Application: Insights on SnF_2 Addition. *ACS Energy Lett.* **2016**, *1*, 1028−1033.

(109) Zhou, Y.; Zhao, Y. Chemical stability and instability of inorganic halide perovskites. *Energy Environ. Sci.* **2019**, *12*, 1495−1511.

(110) Giustino, F.; Snaith, H. J. Toward Lead-Free Perovskite Solar Cells. *ACS Energy Lett.* **2016**, *1*, 1233−1240.

(111) Guerrero, A.; Juarez-Perez, E. J.; Bisquert, J.; Mora-Sero, I.; Garcia-Belmonte, G. Electrical field profile and doping in planar lead halide perovskite solar cells. *Appl. Phys. Lett.* **2014**, *105*, 133902.

(112) Jana, A.; Kim, K. S. Water-Stable, Fluorescent Organic-Inorganic Hybrid and Fully Inorganic Perovskites. *ACS Energy Lett.* **2018**, *3*, 2120−2126.

(113) Zhou, Y.; Zhang, Z.; Fang, Z.; Qiu, M.; Ling, L.; Long, J.; Chen, L.; Tong, Y.; Su, W.; Zhang, Y.; Wu, J. C. S.; Basset, J.-M.; Wang, X.; Yu, G. Defect engineering of metal−oxide interface for proximity of photooxidation and photoreduction. *Proc. Natl. Acad. Sci. U. S. A.* **2019**, *116*, 10232.

(114) Kang, Q.; Wang, T.; Li, P.; Liu, L.; Chang, K.; Li, M.; Ye, J. Photocatalytic Reduction of Carbon Dioxide by Hydrous Hydrazine over Au−Cu Alloy Nanoparticles Supported on $SrTiO_3$/TiO_2 Coaxial Nanotube Arrays. *Angew. Chem., Int. Ed.* **2015**, *54*, 841−845.

(115) Lang, X. J.; Chen, X. D.; Zhao, J. C. Heterogeneous visible light photocatalysis for selective organic transformations. *Chem. Soc. Rev.* **2014**, *43*, 473−486.

(116) Lang, X.; Zhao, J.; Chen, X. Cooperative photoredox catalysis. *Chem. Soc. Rev.* **2016**, *45*, 3026−3038.

(117) Romero, N. A.; Nicewicz, D. A. Organic Photoredox Catalysis. *Chem. Rev.* **2016**, *116*, 10075−10166.